The Pennsylvania State University

The Graduate School

ANALYSIS OF DEPLETION FACTOR IN THE MARCELLUS SHALE GAS RESERVOIRS

A Thesis in

Energy and Mineral Engineering

by

Tianyuan Wei

Submitted in Partial Fulfillment
of the Requirements
for the Degree of

Master of Science

December 2019

The thesis of Tianyuan Wei was reviewed and approved* by the following:

Mort D. Webster
Professor of Energy Engineering
Associate Department Head for Graduate Education
Thesis Advisor

Sanjay Srinivasan
Professor of Petroleum and Natural Gas Engineering
Chair in Energy and Mineral Engineering

Luis F. Ayala H.
Professor of Petroleum and Natural Gas Engineering

*Signatures are on file in the Graduate School

ABSTRACT

The rule of capture has been applied in the development of oil and gas since the first U.S. commercial oil well drilling in Pennsylvania in 1859 (Kramer and Anderson, 2005). The capture rule recognizes that the first party taking possession of the oil or gas has the right to those hydrocarbons even though the party might unintentionally extract some oil or gas that originally resided under the neighbors' lands. Many past legal cases applied the capture rule because of the migratory property of oil or gas, which is analogous to percolating water.

Oil and gas development in shale formations, now increasingly common, are more complex because of different geological properties and different production technologies. The trespass rule was recently applied in Briggs v. Southwestern Energy 184 A.3d 153 (PA, 2018). Based on the rule of trespass, producers are required to pay adjoining landowners for any shale gas captured from their property (Lueck, 1995). The trespass rule asserts that valuable natural gas is locked in unconventional shale reservoirs. It is the hydraulic fracturing conducted by producers rather than the naturally occurring pressure change in reservoirs that makes the shale gas become migratory.

Whether to apply the capture rule or the trespass rule in the context of shale gas development depends in part on the answer to an important question: can we accurately measure the quantity of trespassed natural gas in shale reservoirs? If the cost of measuring the quantity of gas extracted from neighboring land is of the same magnitude as the value of the trespassed gas, it would support the argument for using the capture rule. The Marcellus shale reservoir is used as a case study. I investigate this question by simulating the reservoir flows and projecting the natural gas flow from different types of adjoining land to the wellbore. Because there are large uncertainties about geological properties in any formation, I perform uncertainty analysis to quantify the uncertainty in gas migration amount from each location.

I find that the transaction fees and the cost of petroleum engineering analysis are likely to be greater than the value of trespassed gas, and therefore conclude that the rule of capture should be applied in the Marcellus shale gas development. In other words, considering hydraulic fracturing of shale gas as a trespass action is not justified.

TABLE OF CONTENTS

LIST OF FIGURES

LIST OF TABLES

NOMENCLATURE

A	Block area, ft^2
b	Fracture aperture half width, ft
B_g	Gas formation volume factor at the later time, ft^3/scf
B_{gi}	Initial gas formation volume factor, ft^3/scf
BHP	Bottom-hole pressure, psi
C	Proportional constant in cubic law, $(fts)^{-1}$
CFC	Cumulative fractional contribution of depletion factor, %
CMG	Computer modeling group
CV	Coefficient of variation, %
D	Flow conduit length, μm
DF	Depletion factor, %
DK-LGR	Dual permeability model with the Local Grid Refinement blocks
E	East
FC	Fractional contribution of depletion factor, %
g	Acceleration of gravity, 32.17 ft/s^2
GIP	Gas in place, scf
h	Block height, ft
IGIP	Initial gas in place, scf
J1	Natural fracture joint set 1
J2	Natural fracture joint set 2
K_f	Hydraulic conductivity, ft/s
Kn	Knudsen number
L	Length of fracture, ft
N	North
p	Block pressure, psi
P	Pore pressure, psi
q	Flow rate. ft^3/s

r_e	Outer radius, ft
r_w	Wellbore radius, ft
std	Standard deviation of depletion factor, Mscf
S	South
S_g	Gas saturation at the later time
S_{gi}	Initial gas saturation
SRV	Stimulated reservoir, ft^3
t	Simulation times
T	Reservoir temperature, °R
w	Width of fracture, ft
W	West
x	Coordinates in the horizontal wellbore direction, ft
y	Coordinates in the fracture propagation direction, ft
z	Compressibility factor

Greek letters

α	Bigot factor
μ	Fluid viscosity, cP
σ	Total stress, psi
σ_{eff}	Effective stress, psi
σ_H	Maximum horizontal stress, psi
σ_h	Minimum horizontal stress, psi
σ_v	Vertical stress, psi
ρ	Fluid density, lbm/ft^3
λ	Mean free path of molecules, μm
ϕ	Porosity
Δh	Hydraulic head drop, ft

Subscript

e	Outer
eff	Effective
g	Gas
h	Minimum horizontal
H	Maximum horizontal
i	Initial
v	Vertical
w	Wellbore

ACKNOWLEDGEMENTS

I would like to give my best appreciations to my graduate advisor Dr. Mort D. Webster for his continuous help and valuable support. He teaches me how to work on the research step by step. Thinking independently and asking actively are two powerful weapons he gives me to walk through the challenging parts of the thesis. I also want to extend my appreciations to the members of my thesis committee, Dr. Sanjay Srinivasan and Dr. Luis F. Ayala H. for contributing their expertise and insights along the way.

I would also like to give my gratitude to Dr. Qian Sun for his valuable help in the advices on the gas formation volume factor calculation. His expertise in reservoir simulation and gas well production helped me to overcome the challenges of data evaluation process. I would like to thank my wonderful colleagues and friends at Penn State. They bring me support and happiness through this whole two-and-a-half-year graduate life.

Finally, I wish to express my deep thanks to my parents for their continuous support and encouragement. Thank you for raising me up and educating me throughout my life.

Chapter 1

Introduction

1.1 Marcellus Shale Background

The Marcellus shale is located in the Appalachian basin. Today, multiple Marcellus shale gas developments are taking place in the states of Pennsylvania, New York, Ohio and West Virginia. Marcellus shale plays in Pennsylvania are present in Lycoming County, Fayette County, Wayne County and Wyoming County (Belvalkar and Oyewole, 2010). The Marcellus shale could contain as much as 500 trillion cubic feet (TCF) of gas in place and 50 TCF of recoverable gas (Engelder and Lash, 2008).

The Marcellus shale covers an area greater than 34 million acres and has black organic rich section longer than 50 feet. However, the Marcellus shale has poor physical properties. Core analysis shows that the Marcellus shale has 9.28% average porosity and 0.0196 md mean permeability (Soeder, 1988). Thus, efficient gas production in the Marcellus shale requires stimulation technologies such as hydraulic fracturing and steam injection. The hydraulic fracture stimulation injects fracturing fluid with high pressure at the bottom hole and results in fracture geometry deformation. Induced fractures in shale rock formation greatly enhance the flow capability of natural gas and improve the natural gas recovery.

1.2 Study Problem

This thesis examines the problem of whether or not to apply the rule of capture to shale gas development. The capture rule recognizes the gas possessory rights in the party that first brings the natural gas to the surface. Natural gas, which has a fugacious nature, is similar to percolating water

(Kramer and Anderson, 2005). When buried underground, gas tends to migrate. Gas cannot be definitively specified as existing under a specific plot of land. Thus, natural gas belongs to the landowner as long as the gas resides under the land, but when the natural gas escapes into other lands and becomes subject to other landowners, the title of the natural gas is changed. Based on the capture rule, a producer possesses the title to the gas produced from the wells drilled under the producer's land, even if some of this gas migrates from neighbors' lands.

However, the case of Briggs v. Southwestern Energy in 2018 stated that the percolating water analogy of natural gas is not applicable to shale gas development. This case concluded that producing shale gas from adjoining lands is a trespass action (Lueck, 1995). In other words, the producers should pay for any natural gas captured from land belonging to other parties. The rule of trespass in the Briggs case asserted that the shale gas is locked in the reservoir and cannot flow on its own. It is the hydraulic fracturing conducted by the producers that change the reservoir pressure and make the shale gas become migratory. Thus, the Briggs case determined that the rule of capture did not apply to the shale gas development.

Whether to apply the capture rule to the shale gas development relies largely on a critical question: is it possible to accurately measure the quantity of trespassed gas in the Marcellus shale? Given a specific plot of land, a petroleum engineering analysis on how much gas extracted from that land can be conducted. If the analysis cost is of the same magnitude as the value of trespassed gas from the land, the rule of capture should be applied. In contrast, if the rule of trespass is applied, the large uncertainties about the geological engineering properties should be analyzed.

1.3 Adjoining Land Properties

Two critical properties, the stimulated reservoir volume (SRV) and the distance from wellbore, determine the amount of production from hydraulic fracturing for a given location. In the simulation, I explore the implications for three distinct land situations associated with the SRV and the wellbore:

1) Close to the wellbore and below which is the SRV region.

2) Adjacent to the wellbore while out of the SRV region.

3) Distant from the wellbore and the SRV region.

In the petroleum engineering analysis, three plots of land are selected and the extracted natural gas amount is estimated for each. Because of the large uncertainty in geological and engineering properties, I perform an uncertainty analysis using Monte Carlo simulation to quantify the uncertainty in the amount of gas extracted.

Chapter 2 of this thesis reviews the literatures about the Marcellus shale properties and explains the engineering models in the simulation. Chapter 3 presents the methodology used in the simulation analysis. Chapter 4 explains the numerical reservoir base model and examines the initial results. Chapter 5 presents the sensitivity analysis. Chapter 6 shows the uncertainty analysis work and considers the economic costs of producers when the trespass rule is applied. Chapter 7 shows the conclusions of my study.

Chapter 2

Literature Review

2.1 Shale Gas Reservoir

Natural gas constitutes an increasing share of worldwide resource consumption, and combustion of natural gas produces nearly half of the carbon dioxide from all conventional fossil fuels. Previous studies have shown that shale formations store a huge amount of natural gas. In the past, shale reservoirs were seen as unconventional reservoirs because exploiting shale formations required advanced drilling and completion expertise, which had very high cost. However, recent innovations in petroleum production technology have made it possible to drill for the natural gas stored in unconventional reservoirs such as shale gas reservoirs.

To understand a shale gas reservoir, the rock properties and the common geological structures of this unconventional reservoir are important to consider. Shale is a clastic sedimentary rock made up of clay minerals and quartz. Low permeability is the main characteristic. Shale rock is difficult for fluid to pass through and traditionally serves as the main cap rock of conventional reservoirs. In addition, nearly 90 percent of organic matter inside sedimentary rocks is stored in shales and mudrocks. This organic matter is what forms natural gas and oil. Thus, natural gas can be produced and retained in shale formations.

To produce gas from these formations requires a stimulation method to open the shale formations and force the natural gas come out, since that gas is locked in the shale. In recent years, the technologies for stimulation and well completions have improved greatly. In particular, multi-stage hydraulic fracturing and large-volume slickwater injection can generate an artificial fracture system in shale formations and result in fracture propagations (Walton and McLennan, 2013).

Those stimulated fractures serve as the path for natural gas to flow towards the wellbore. Resource companies can now produce shale gas on a large commercial scale and its production is economic.

2.2 Naturally Fractured Reservoir

Natural fractures commonly exist in hydrocarbon reservoirs. Stress conditions and formation geomechanics properties built the natural fractures in oil and gas reservoirs. However, it is not easy to interpret the structures of those natural fractures. Regional fractures consist of tiny fractures and some large-scale fractures. Large fractures control the flowing capability of hydrocarbons during the production process. (Lorenz et al., 1996).

In the geology context, rock breaks under shear forces or breaks under tensions can cause rock fractures (Handin and Hager, 1957). The breaks under shear forces generate faults while the breaks under tensions yield a high density of joints (Pollard and Aydin, 1988). At the depth of the Marcellus shale, compressive stress is the main kind of stress and the tensions play a critical role in rock. Thus, extensive joints appear in the Marcellus shale.

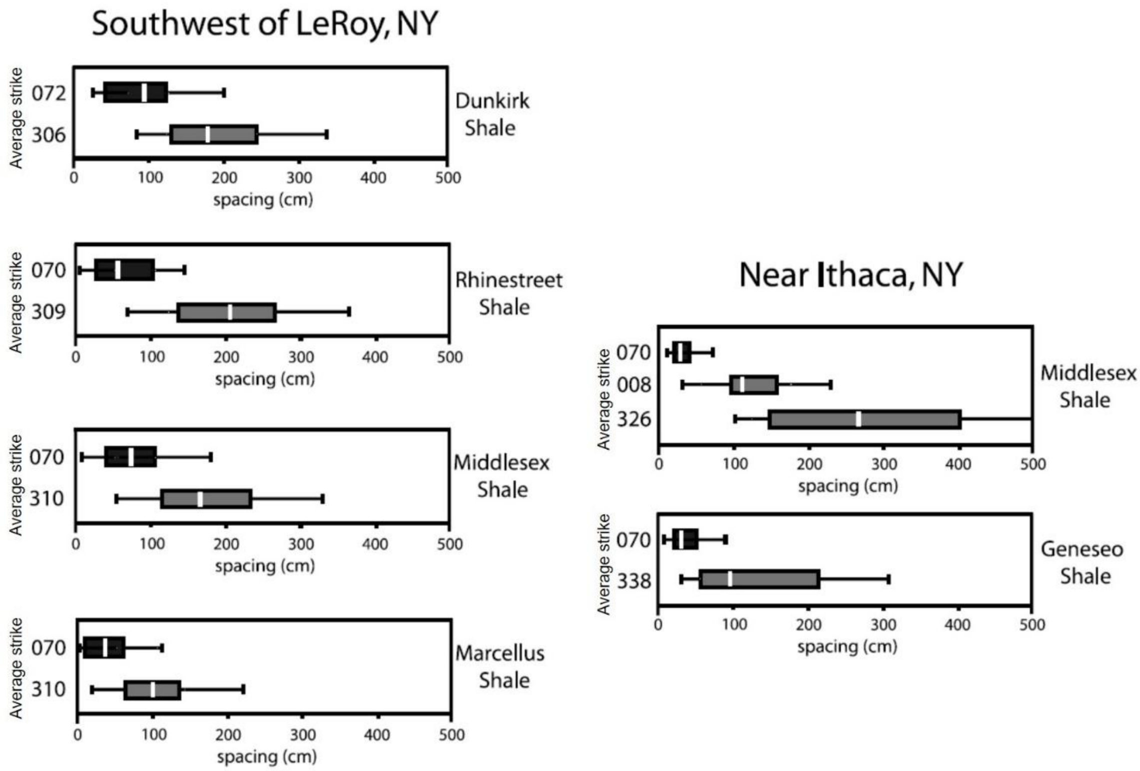

Figure 2-1. Joint Density of J1 Sets and J2 Sets (Engelder et al., 2009)

Three types of natural joint sets occur in the Appalachian Basin which are referred to as J1, J2 and J3 sets (Engelder et al., 2009). These three joint sets are the main natural fractures in this region. From the observation of outcrops, the Marcellus shale commonly carries two joint sets: J1 and J2 joints. Figure 2-1 shows the fracture spacing and the average strikes of J1 and J2 sets. In these box -and-whisker plots, the black boxes represent the J1 joints and the grey boxes represent the J2 joints.

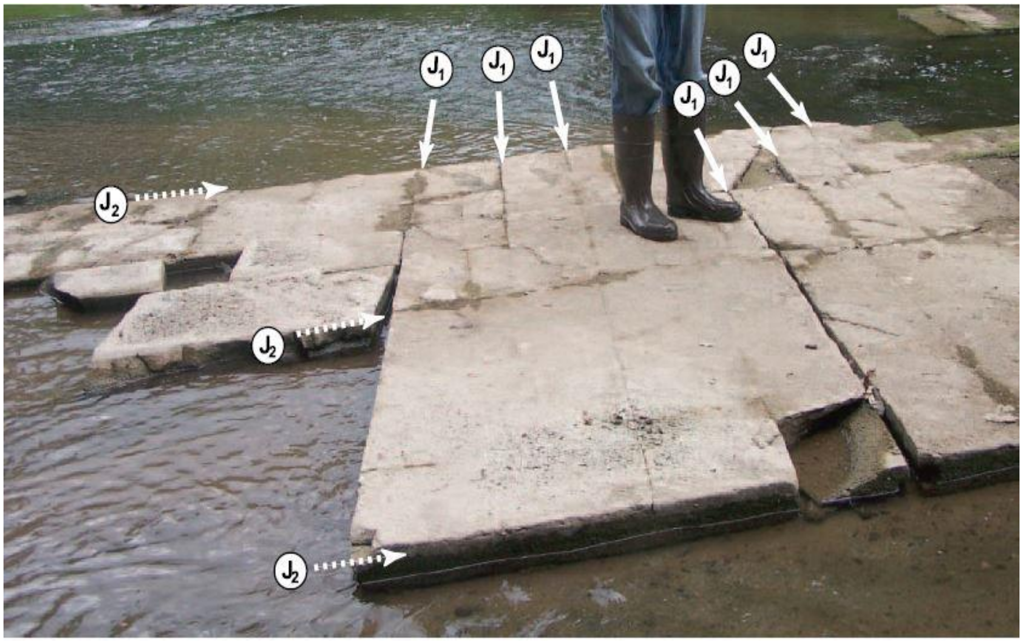

Figure 2-2. J1 and J2 Joints in the Marcellus Black Shale (Engelder et al., 2009)

The J1 sets mostly appear in black shales, and the J2 sets mostly appear in grey shales and siltstones. From Figure 2-2, the set of J1 takes the strike of the east-northeast. Additionally, the earlier J1 sets are mostly crosscut by the later J2 sets (Figure 2-2). The J2 joints run to the north-northwest direction and are more widely spaced than the J1 joints. In the Marcellus shale, the J1 sets have one-foot mean fracture spacing while the average fracture spacing of the J2 sets is three feet. The maximum compressive normal stress has a parallel direction to the strikes of the J1 joints (Engelder et al., 2009). Further, the J3 joints, which have the east-northeast strike, are the neotectonics fractures caused by the contemporary tectonic stress.

2.3 Hydraulic Fracturing Stimulation

From the discussion on the gas reserves, shale formations store a huge amount of locked natural gas. In addition, systematic natural fractures propagate extensively through shale formations. To extract the natural gas in deep reservoirs, artificial fractures are commonly generated to connect the gas well to the natural fracture network. Here is the hydraulic fracturing technology. Once the perforations have been completed, those perforation holes connect the rock and the wellbore successfully. However, those short perforation holes cannot have access to the whole natural fracture network. The hydraulic fracturing technology makes it possible to create longer and wider artificial fractures by pumping a mixture of water, sands and other chemical materials. Pressurized water leads to a fracture growth. The injected sands stay in the rock and keep the stimulated fractures open. Thus, the trapped natural gas will flow to the wellbore and become extracted. Finally, the fracturing fluid will be recycled for other fracturing operations or disposed of in a safe manner.

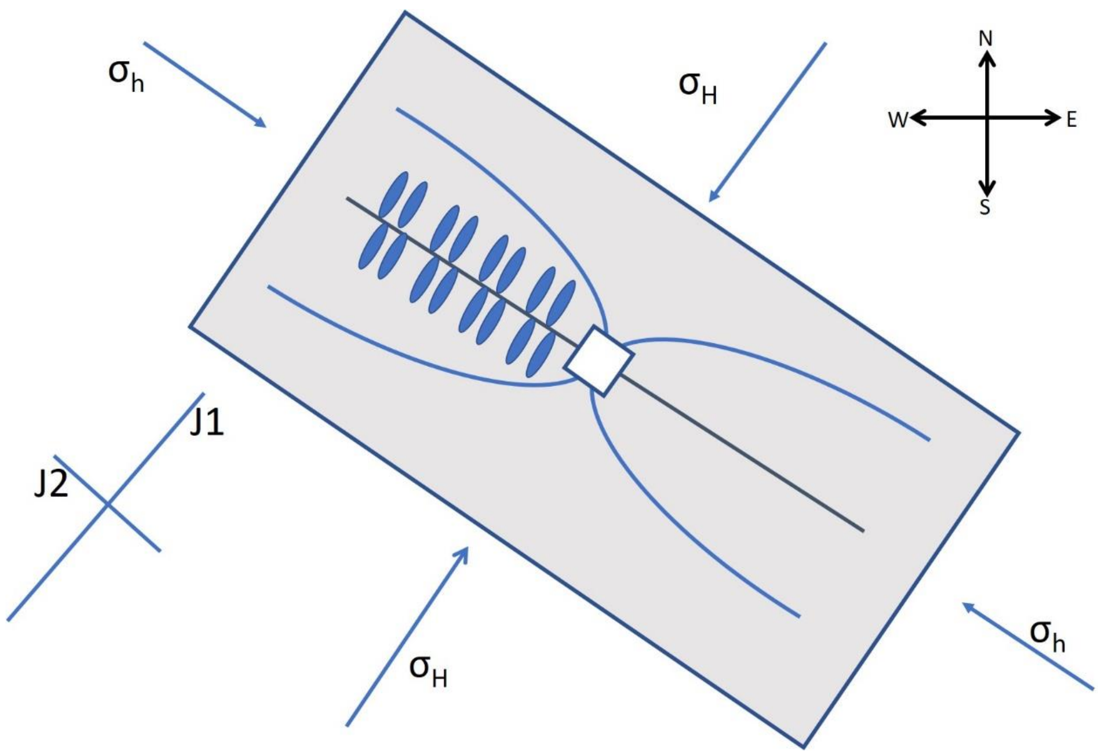

Figure 2-3. Top View of Half Hydraulic Fracturing Stimulation

From the geomechanics viewpoint, the fracture propagation direction should be vertical to the minimum horizontal stress axis. The Appalachian Basin is experiencing a tectonic stress field whose maximum horizontal compressive stress orientation is the east-northeast (Sbar and Sykes, 1973). Further, the contemporary hydraulic fracturing completions, whose target is the Marcellus shale, are orientated to the east-northeast (Figure 2-3). Thus, the stimulated fractures run the east-northeast and drain the more pervasive J2 joints under the tectonic stress influence. The natural gas production can be enhanced greatly by linking the naturally unhealed fractures to the wellbores.

2.4 Hydraulic Fracture Models

A model forecasting the stimulated fracture propagation is necessary before starting the stimulation procedure. Here are the model building steps. First, well tests provide matrix permeability data for the model. Later, this model needs to consider matrix-matrix flow, matrix-fracture flow and fracture-fracture flow. Additionally, building appropriate models requires the consideration of in-situ stresses and fracture mechanics parameters.

2.4.1 In-Situ Stress

In-situ stress evaluation is the foundation of reservoir geomechanics study. Whether a fracture would occur depends on the difference between the rock strength and the effective stresses. If the effective stresses exceed the rock strength, failures will be generated inside the rock. In common conditions, the rock strength is measured in lab experiments. In-situ stresses are commonly recorded throughout rock strength measurements. The measured rock strength is called the unconventional compressive strength. In-situ stresses include vertical stress (overburden stress), minimum horizontal stress and maximum horizontal stress (Figure 2-4).

The relationship between the total pressure and the effective formation pressure is shown below:

$$\sigma = \sigma_{eff} + \alpha P \tag{1}$$

Where σ is the total stress, σ_{eff} is the effective stress, P is the pore pressure and α is the Biot factor. During hydrocarbon production, pore pressure will decrease. This phenomenon accounts for the effective stress increase when the overburden stress (total stress) is still.

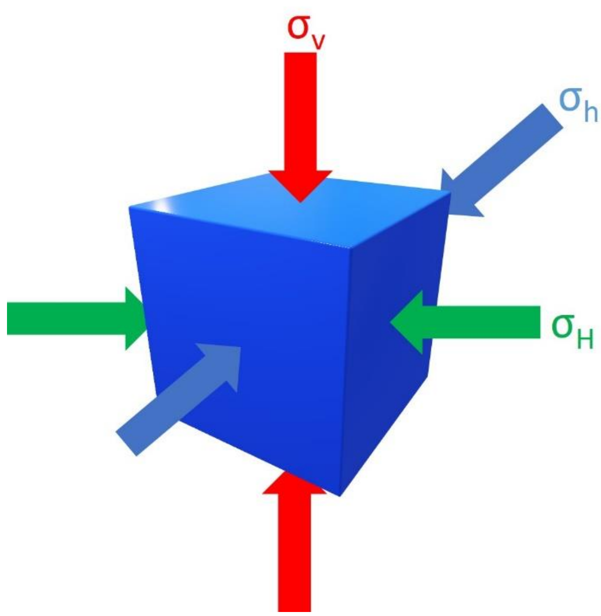

Figure 2-4. Underground In-situ Stresses

Figure 2-4 shows the in-situ stresses in underground conditions. Where σ_v is the vertical stress (or overburden stress), σ_H is the maximum horizontal stress, σ_h is the maximum horizontal stress. Units for parameters above are all psi.

Failures can lead to poor stimulation outcomes and result in unsteady gas productions. Petroleum industry pays a great attention to in-situ stresses. Characterizing in-situ stress magnitudes and orientations is the critical step in the reservoir simulations (Belvalkar and Oyewole, 2010).

2.4.2 Hydraulic Fracture Model

Hydraulic fracture stimulation applies a high fluid pressure at bottom hole and deform fracture geometries in order to improve production performances. Hydraulic fracturing technology includes two steps. Injecting fluid into formations is the first step. The pressure of injected fluids should be higher than the breakdown pressure of formations. Then, cracks start to propagate. The following step is the fracture stabilization. Injecting the viscous fluid mixed with proppants leads to fracture growths and moves the injected proppants to the designed locations. From the geomechanics viewpoint, three factors (the injected fluid properties, in-situ stresses and rock parameters) determine the geometry of stimulated fractures. Two-dimensional hydraulic fracture models, Perkins-Kern-Nordgren (PKN) model and Geertsma-de Klerk (GdK) model, discuss these three factors and characterize the geometry of fractures.

The vertical plane strain assumption is used by Perkins and Kern to predict the hydraulic fracture width. The PK model is used when the formation confinement is high and the fracture length is much greater than the fracture height. The displacements of the cross planes are independent of the z axis. Further, PK model provides width assessment approaches for horizontal fractures and vertical fractures. Fracture width outcomes are not sensitive to the change of rock geomechanics properties such as Young’s moduli (Perkins and Kern, 1961).However, adjusting surface pumping rates influences the fracture width greatly.

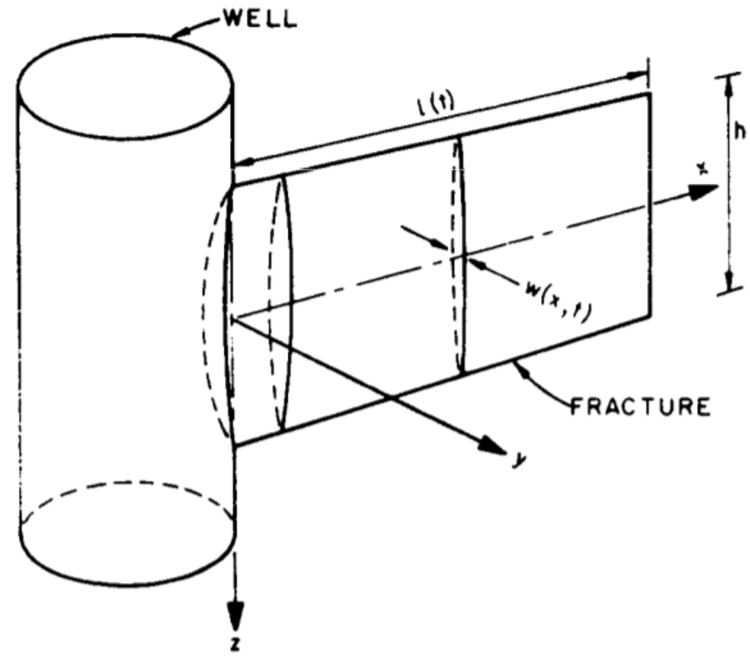

Figure 2-5. Fracture geometry in PKN (Nordgren, 1972)

However, the PK model assumes that the maximum fracture is not changed during the fracture propagation process. Because of that, predictions from PK model is not convincing because such assumption is different from physical conditions. Nordgren adds the fluid flow equation to the PK model. Thus, the maximum fracture width will decrease along the fracture and the Perkins-Kern-Nordgren (PKN) model is further developed (Nordgren, 1972). The schematic view of the PKN model is shown in Figure 2-5. The cross section of the PKN fractures is elliptical. Moreover, the Carter II equation adds the fluid leak-off coefficient to develop the PKN model. Thus, the following Perkins-Kern-Nordgren-Carter (PKN-C) model considers the maximum fracture width changes along the fracture propagation direction and the fluid loss effects.

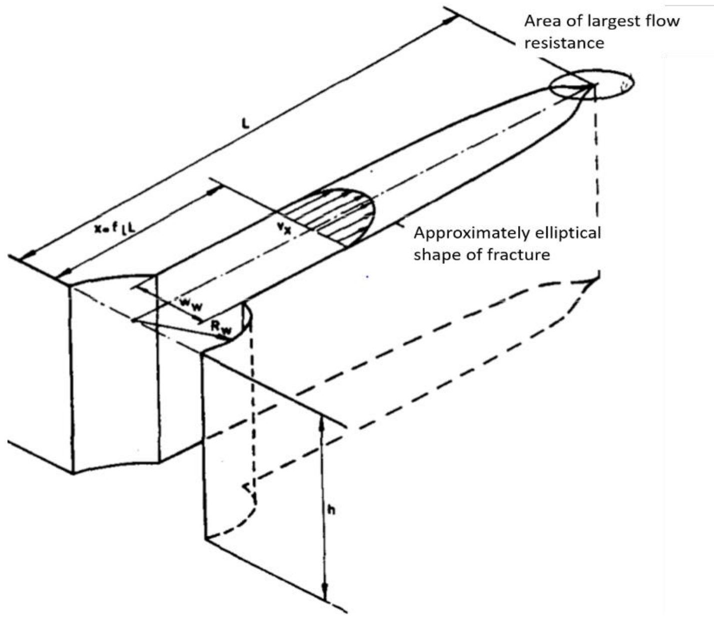

Figure 2-6. Schematic View of GdK Model (Geertsma and de Klerk, 1969)

Another two-dimensional model is the Geertsma and de Klerk (GdK) model. The GdK model uses the plane stress assumption which means that all stress components are independent of the vertical direction. Locations with different heights have the same stress. Considering the fluid efficiency in fractures having small length-height ratios, the GdK model is suitable for tall and short fractures (Figure 2-6).

2.5 Flow inside Porous Media

After understanding the void spaces and the fracture systems inside shale formations, attentions need to be paid to fluid dynamics and the interactions between the fluid and the porous media. The Marcellus shale formation is enforced to high compaction. Given this, most of the grains of the Marcellus Shale are micrometer-sized or nanometer-sized (Moghaddam and Jamiolahmady, 2016). In the geological context, the nanometer porous radius and the micrometer porous radius are close to the mean free path of the natural gas molecules. In contrast, natural joints and stimulated fractures are the large-scale flowing channels inside the Marcellus shale formations.

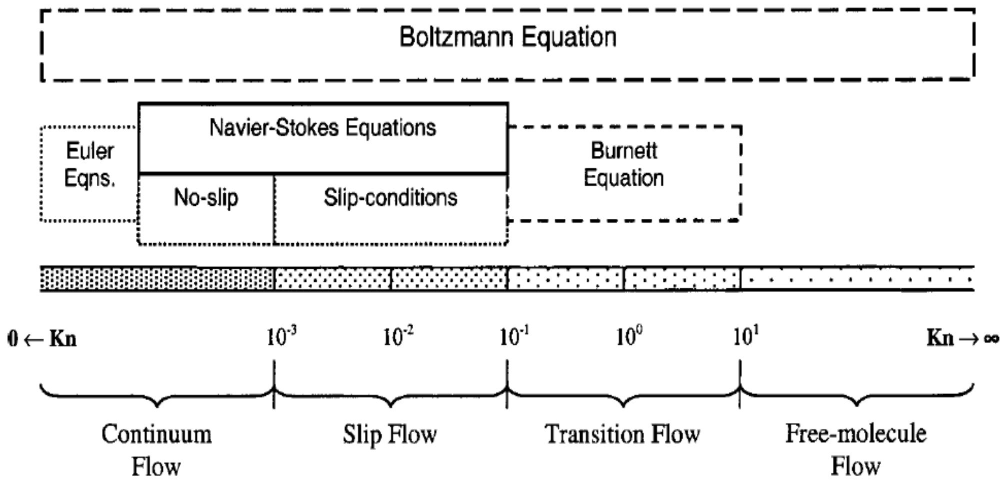

Figure 2-7. Knudsen Number Regimes (Roy and Raju, 2003)

The complex flow conduit system in the Marcellus shale results in multiple shale gas flow regimes including continuum flow, slip flow, transition flow and free-molecule flow (Figure 2-7). Previous studies have shown that the Navier-Stokes equations with different boundary conditions can be used to predict the flow capabilities in shale formations.

A critical parameter, the Knudsen number (Kn), is commonly used to determine the flow type:

$$\mathrm{Kn} = \frac{\lambda}{D} \tag{2}$$

where λ is the mean free path of molecules and D is the flow conduit length.

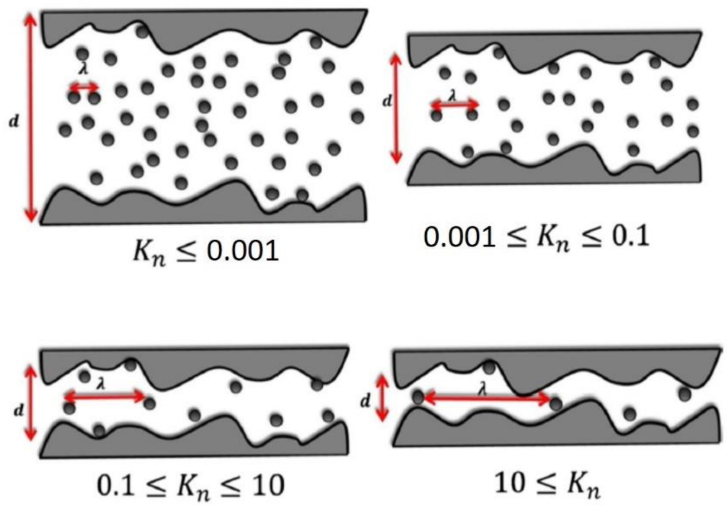

Figure 2-8. Schematic View of Different Flow Types (Moghaddam and Jamiolahmady, 2016)

Figure 2-8 shows the schematic view of different flow types and the corresponding ranges of different Kn numbers.

2.5.1 Flow in fractures and Macroscale Systems

When the Kn is smaller than 0.001, the whole gas flow is the continuum flow which is also referred to as the Darcy's flow. This continuum gas flow is seen as a continuous mass rather than discrete gas molecules. To characterize this continuum flow, the Navier-Stokes equation with no slip boundary conditions is commonly used. However, three assumptions of the continuum flow are made:

1) The flowing gas has the Newtonian viscosity.

2) The flow conduit length is much greater than the mean free path of gas molecules.

3）The whole flowing process satisfies the thermodynamic equilibrium.

2.5.2 Flow in Nanoscale and Microscale Systems

When gas flows through nanoscale or microscale systems, Kn is greater than 0.01. Given the flow regimes division based on the Kn, flow regimes such as slip, transition and free-molecule will exist in shale formations. In other words, if the conduit length gets smaller, not only the collisions between gas molecules but also the collisions between gas molecules and the rock wall need to be considered (Moghaddam and Jamiolahmady, 2016).

For the Kn number greater than 0.001 and smaller than 0.1, the flow near the rock wall is the slip flow regime. The continuum flow boundary condition is still valid inside the gas bulk. However, new slip boundary conditions should be used in the Navier-Stokes equation in order to describe the flow paths near the rock wall. When the Kn is between 0.1 and 10, flow is in the transition flow regime. The transition flow will switch between the slip flow and the free molecule flow. For the Kn greater than 10, the free-molecule flow dominates the flow regime.

When the Kn is greater than 0.1, the conventional characterization of gas flow based on the Navier-Stokes equation without slip boundary conditions is invalid. Most gas flow needs to be predicted using other statistical methods. Common statistical methods include the molecular dynamic method, the direct simulation Monte Carlo method and the linearized Boltzmann equation method. However, the same problem for those simulation methods is the long running time.

Chapter 3

Problem Statement

When well starts to produce natural gas, reservoir pressures will have reductions and those gas would flow from the high-pressure locations to the wellbore. Natural gas not only flows from producers' leased lands but also flows from adjoining areas. In some unconventional resource development cases, the rule of trespass is applied which means that producers have to pay for the resources extracted from other landowners' lands. A model that can estimate the quantity of natural gas having been extracted from a specific area is needed to calculate the money should be paid by those producers.

Determining the extracted gas is challenging in unconventional reservoirs. Unconventional reservoirs have more complex flows and more intricate resource distributions. Additionally, how certain the estimate is needs to be answered. The trespassed gas calculation should consider the effects of some petroleum engineering factors such as matrix permeability, fracture conductivity, pore pressure and bottom-hole pressure. Those engineering factors adds uncertainties to the estimated amount of trespassed gas. From the viewpoint of producers, uncertainties of estimates would greatly affect drilling incentives.

The objective of my work is to develop a model being able to calculate the amount of natural gas having been taken out from a chosen area. Further, sensitivity analysis is performed to evaluate the influence of the engineering factors. In addition, sufficient simulation outcomes are used to calculate the uncertainties of the estimated results.

To run this model, one needs to put the reservoir depth, porosity, fracture spacing and fracture conductivity into the simulator. The natural gas depletion factor for every block area will be calculated. Given the landowner's area, my model will calculate the gas produced from that area and determine how accurate the estimated results are.

Chapter 4

Model Development

4.1 Model Characteristics

In order to calculate how much natural gas having been extracted from landowner's area, volumetric calculations will be performed in a numerical reservoir model and natural gas depletion factor (DF) can be computed. This model development chapter discusses the reservoir model design and the physics property assumptions in my model.

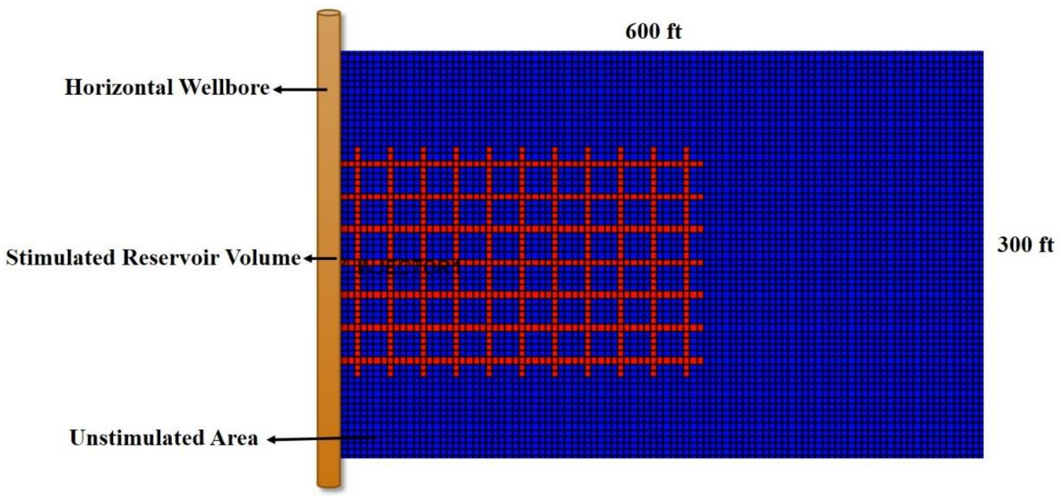

Figure 4-1. Schematic of Half Stimulated Reservoir Volume

The Black oil model (Trangenstein and Bell, 1988) characterizes a system whose gas can exist in solution in the oil phase and whose oil can exist in the gas phase. Dry gas reservoir, which only deals with the gas phase flow in reservoirs, is a special case of the black oil model. In order to simulate the gas flow, a two-dimensional dry gas reservoir is developed in a simulation software called Computer Modeling Group (CMG). This model is designed to conduct the studies on the amount of shale gas having been extracted from an area of 180 thousand square feet.

Figure 4-1 shows the schematic view of half stimulated section of one fracture stage. A hydraulically fractured horizontal well is drilled at the reservoir center. One assumption is that the fractures have equal extending distances on two sides of the wellbore. Red grids represent the stimulated fracture network. This simulator only deals with half of the reservoir area.

The shale gas reservoir is set as gas-saturated in the first step. Injecting fracturing fluids makes the reservoir become hydraulically fractured. This simulator has a 180 thousand square feet drainage area and extends to two perpendicular directions. The first direction is the wellbore direction. The second direction is the hydraulic fracture propagation direction. The reservoir input parameters are shown in Table 4-1. Most parameters in Table 4-1 are kept constant in the simulation. The pore pressure gradient is the formation pressure increase when the vertical depth increases one foot.

Matrix porosity is the primary porosity produced by geological formation deformations. Fracture porosity is the secondary porosity resulted from tectonic fracturing inside rocks. The porous spaces in shale formations commonly have two classes of porosity: matrix porosity and fracture porosity. A natural fractured reservoir can be idealized into a combination of discrete blocks with matrix porosity coupled by fracture porosity, which is called the dual porosity model (Warren and Root, 1963).

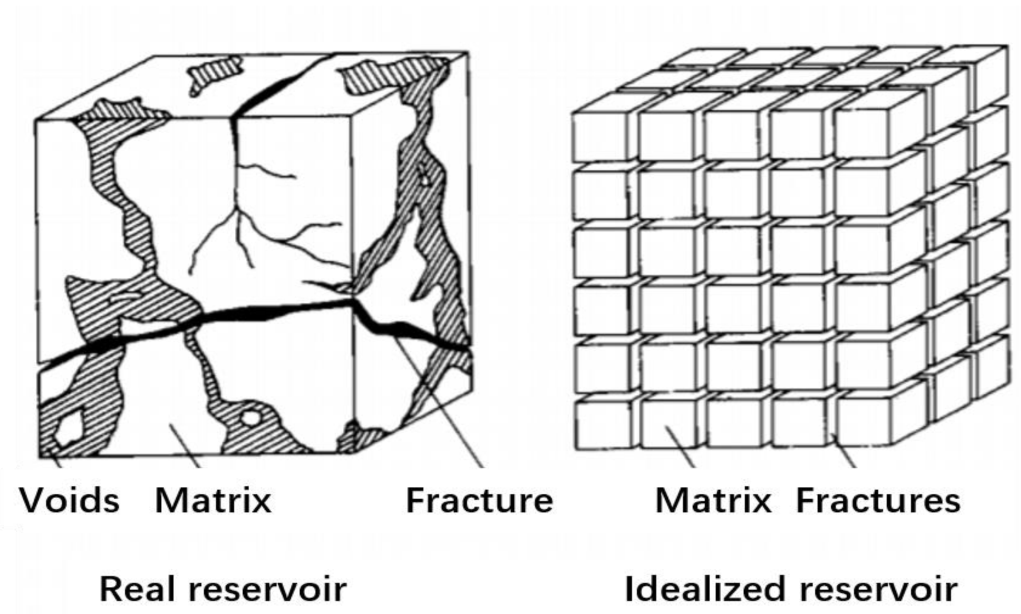

Figure 4-2. Heterogeneous porous model (Warren and Root, 1963)

The dual porosity model and the dual permeability model are used in the simulations of naturally fractured reservoirs. The matrix porosity system typically appears in sandstone or limestone systems. The matrix porous space is intergranular and contributes greatly to the pore volume of shale formations while no fluid flows through those matrix pores. Fracture porosity is caused by fracturing and contributes significantly to the flow capability inside reservoirs. In this heterogeneous porous model, an independent fracture network is superimposed on each matrix block (Figure 4-2). The fracture system flow, including the fracture-fracture flow and the matrix-fracture flow, is the primary type of flow in reservoirs.

When compared with the dual porosity model, the dual permeability model adds the fluid flow between different matrix blocks. Every matrix block is connected to both the surrounding fracture blocks and the surrounding matrix blocks. Then gas can flow through both the fracture systems and the matrix blocks. The matrix to matrix flow is very important when the fracture connectivity is oriented to a designed direction.

The simulated reservoir is built by a grid system made up of the SRV block region and the matrix block region. Each block in the SRV region is divided into 5 × 5 smaller subdomains (Abdelmoneim et al., 2012). Further, the pseudo-fracture fairways are built in each SRV block to represent the effective permeability and the effective porosity of a fracture with a 0.001 feet width. In other words, the fracture porosity is zero in the subdomains not set as the fracture fairways. Those regions only have the designed matrix porosity. This method is called a dual permeability model with the Local Grid Refinement blocks (DK-LGR).

The Forchheimer correction factor is used to simulate the non-Darcy flow in those fracture fairways. However, this DK-LGR method is not suitable for simulating the reservoirs with the matrix permeability greater than 0.01 md. In other words, the DK-LGR method can produce reliable simulation results for fractured shale gas reservoirs.

Table 4-1. Reservoir Simulation Inputs

Reservoir Simulation Inputs	Numerical Values	Citation
Drainage Area, ft^2	180,000	(Engelder et al., 2014)
Stimulated Length, feet	500	(Mayerhofer et al., 2011)
Stimulated Width, feet	200	(Ayers et al., 2012)
Thickness, feet	300	(Cipolla et al., 2009)
Reservoir Block Size	120 × 60	(Cipolla et al., 2009)
Study Depth, feet	9,000	(Cipolla et al., 2009)
Well Radius, feet	0.125	(Mukherjee and Economides, 1991)
Fracture Spacing, feet	3 × 1	(Cipolla et al., 2009)
Maximum Surface Gas Rate, standard cubic feet / day	10,000	(Osholake, 2010)
Matrix Porosity, %	3	(Walton and McLennan, 2013)
Fracture Porosity, %	0.0025	(Izadi et al., 2014)
Initial Gas Saturation, %	80	(Cipolla et al., 2009)
Reservoir Temperature, Deg F	275	(Izadi et al., 2014)
Matrix Permeability, md	0.0001	(Osholake, 2010)
Hydraulic Fracture Conductivity, md-ft	4	(Cipolla et al., 2009)
Bottom-hole Flowing Pressure, psi	2,500	(Cipolla et al., 2009)
Pore Pressure Gradient, psi/ft	0.4	(Walton and McLennan, 2013)

The half-length of artificial fractures in the completed Marcellus shale horizontal wells has a range from 350 feet to 1125 feet (Mayerhofer et al., 2011). Thus, the half-length of the stimulated fractures is set to be 500 feet in our model. As can be found in Figure 2-1 and Figure 2-3, the fracture spacings along the wellbore direction and along the fracture propagation direction are different. This corresponds to the fracture spacing input (3 feet × 1 foot) for the base model in Table 4-1. The 3 feet represents the mean fracture spacing for the J2 joints and the 1 foot is the average fracture spacing for the J1 joints (Engelder et al., 2009).

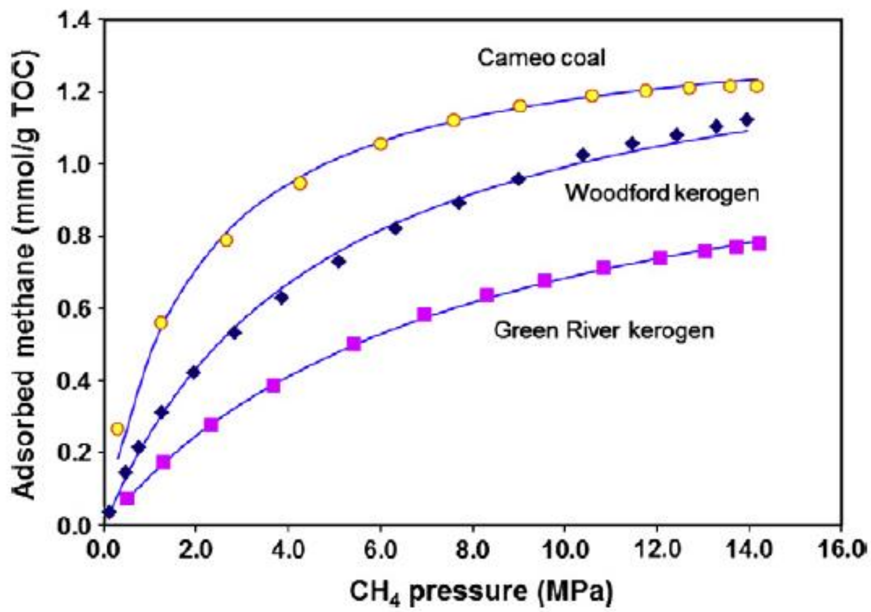

Figure 4-3. Comparison of Sorption Capacity for Three Shale Samples (Zhang et al., 2012)

The adsorption mechanism is that some gas molecules has a tendency to cling to shale formation surfaces. From Figure 4-3, when pressure is higher than 12 MPa, the amount of adsorbed natural gas does not increase greatly with pressure. When pressure decreases to 8 MPa or below, more gas attached to the shale formations will be released from the rock surfaces (Zhang et al., 2012). This phenomenon is called the desorption. Natural gas adsorbed to the formation takes up to 15% of total shale gas reserves.

In the base model, the bottom-hole pressure of the well is kept at 2,500 psi. In order to produce natural gas, the pressure at each location in the simulator is higher than 2,500 psi (17.24 MPa). Thus, the amount of natural gas recovery resulted from desorption mechanisms does not contribute to the gas recovery since the adsorbed gas within the pressure range in the base model is not migratory.

The depletion factor (DF) is the gas extracted volume at the standard condition (60 °F and 14.7 psia) divided by the initial total gas volume at the standard condition (IGIP). Each grid block has a five-feet length and a five-feet width. The depletion factor at each location is obtained by the volumetric calculation:

$$IGIP = \frac{Ah\phi S_{gi}}{B_{gi}} \tag{3}$$

$$GIP = \frac{Ah\phi S_{g}}{B_{g}} \tag{4}$$

$$DF = \frac{IGIP - GIP}{IGIP} \tag{5}$$

where A is the block area, h is the block height, ϕ is the porosity, S_{gi} is the initial gas saturation, B_{gi} is the initial gas formation volume factor, S_g is the gas saturation at the later time and B_g is the gas formation volume factor at the later time.

When the well starts to produce natural gas, the gas saturation at each block will decrease from the initial gas saturation to the gas saturation at the later time. Gas formation volume factor is the ratio of the gas volume at the reservoir condition to the gas volume at the standard condition. The pressure drop changes the initial gas formation volume factor to the gas formation volume factor at the later time. The block area, the block height and the porosity are kept constant throughout the volumetric calculation.

The gas formation volume factors corresponding to different pressures at different locations are calculated by the Soave-Redlich-Kwong (SRK) equation. This SRK equation is an equation of state to calculate the compressibility factor of natural gas. Further, the gas formation volume factor is calculated by the real gas law:

$$B_g = 0.02827 \frac{zT}{p} \quad (6)$$

where Bg is the gas formation volume factor whose unit is ft^3/scf, z is the compressibility factor and T is the temperature whose unit is Rankine Degree.

Table 4-2. Volume Parameters under Different Pressures (Osholake, 2010)

Pressure, psi	Solution Gas-Water Ratio, Standard Cubic Feet / Stock Tank Barrel	Formation Volume Factor of Gas, Cubic Feet / Standard Cubic Feet
414.0	170.93	0.04980
813.2	340.46	0.02523
1212.5	505.15	0.01689
1611.8	669.79	0.01272
2011.0	832.33	0.01024
2410.3	988.73	0.00860
2809.6	1133.34	0.00744
3208.8	1272.65	0.00659
3608.1	1392.22	0.00593
3684.5	1394.05	0.00583

The gas simulation requires the input of formation volume factor data and solution gas-water ratio data. Table 4-2 shows the formation volume factors of gas and the solution gas-water ratios under different pressures.

4.2 Simulation Results of the Base Model

4.2.1 Pressure and Gas Saturation Distribution after 15 Years

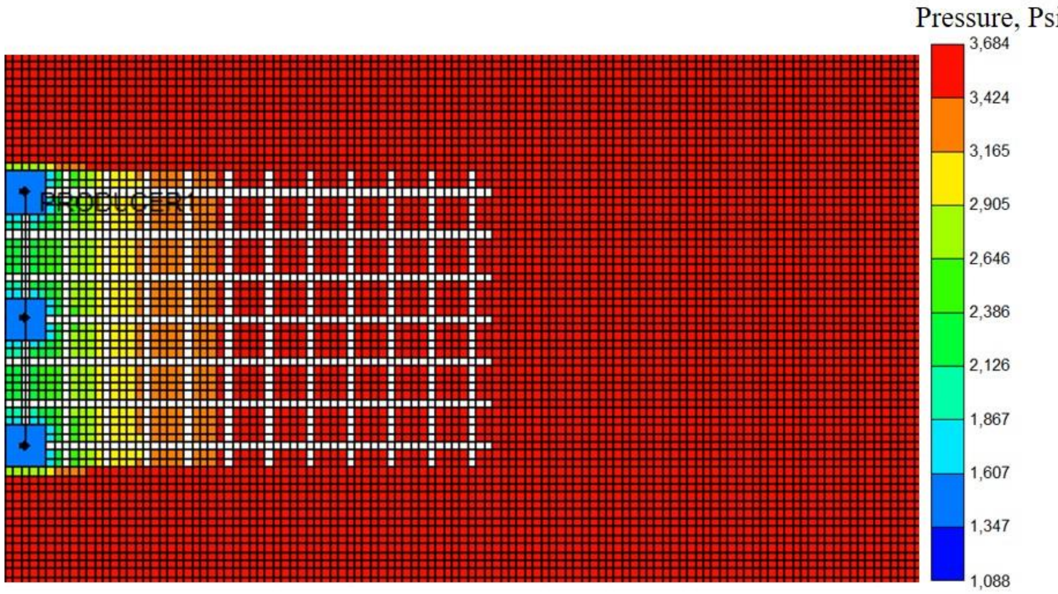

Figure 4-4. Pressures of Each Location in the Reservoir after 15 Years

As the volumetric calculation method has shown, two most important parameters in the model are the pressure and the saturation. Figure 4-4 and Figure 4-5 show the pressure change and the gas distribution when the gas well has produced for 15 years. There are three big grids representing the perforation clusters along the horizontal wellbore. Those three blocks are connected with each other. Thus, natural gas can flow from the lower perforation clusters to the upper perforation cluster and become extracted at the surface. In the CMG software setting, the perforation block cannot be divided into smaller subdomains. This explains why the perforation cluster blocks are bigger than the surrounding blocks.

For the locations outside the stimulated reservoir volume (SRV) region, the pressures do not change too much. The gas outside the SRV region will not flow to the gas well because there is not too much pressure difference. In contrast, locations under the SRV region have lower pressures. Natural gas will flow from high-pressure locations to low-pressure locations (locations close to the wellbore) and those gas will become extracted.

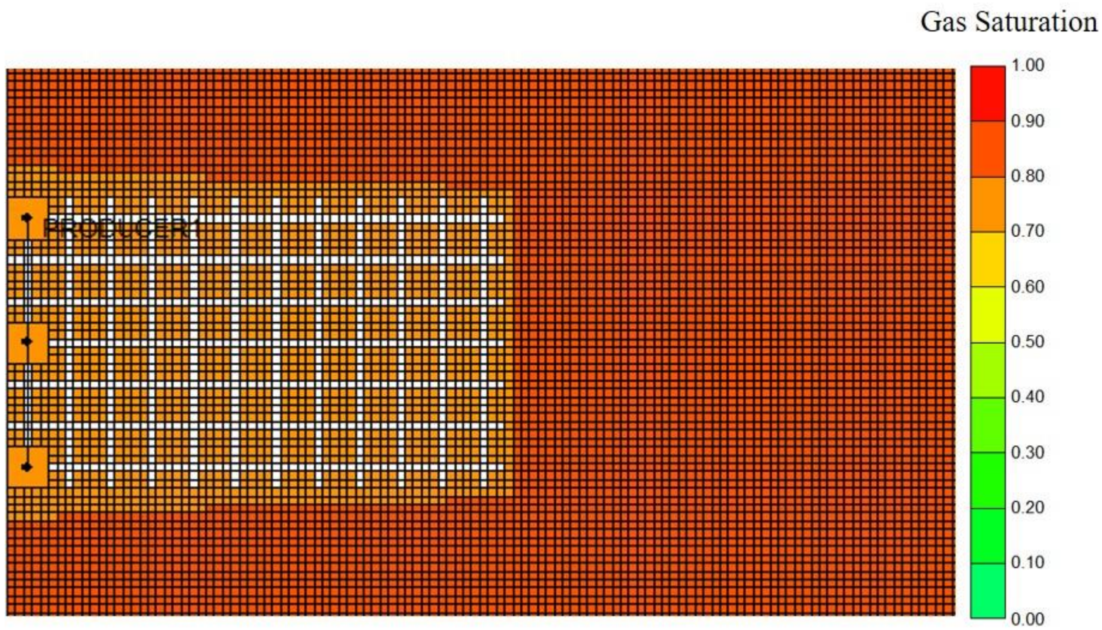

Figure 4-5. Gas Saturation of Each Location in the Reservoir after 15 Years

From Figure 4-5, nearly all the natural gas within the SRV region becomes migratory after 15 years. Gas uses the fracture network as the flow channel and migrates to low-pressure locations. However, the change of gas saturations is small, which means that the ratio of the extracted gas to the total amount of gas is still very low. The low matrix permeability of shale formation results in the small change of gas saturations after 15 years.

4.2.2 Comparison between the Matrix Depletion Factor and the SRV Depletion Factor

When the locations are inside the SRV region, the depletion factors of those locations are referred to as the SRV depletion factors. In contrast, if the locations are in the matrix region (locations with low permeability and low porosity), depletion factors calculated at those locations are called the matrix depletion factor.

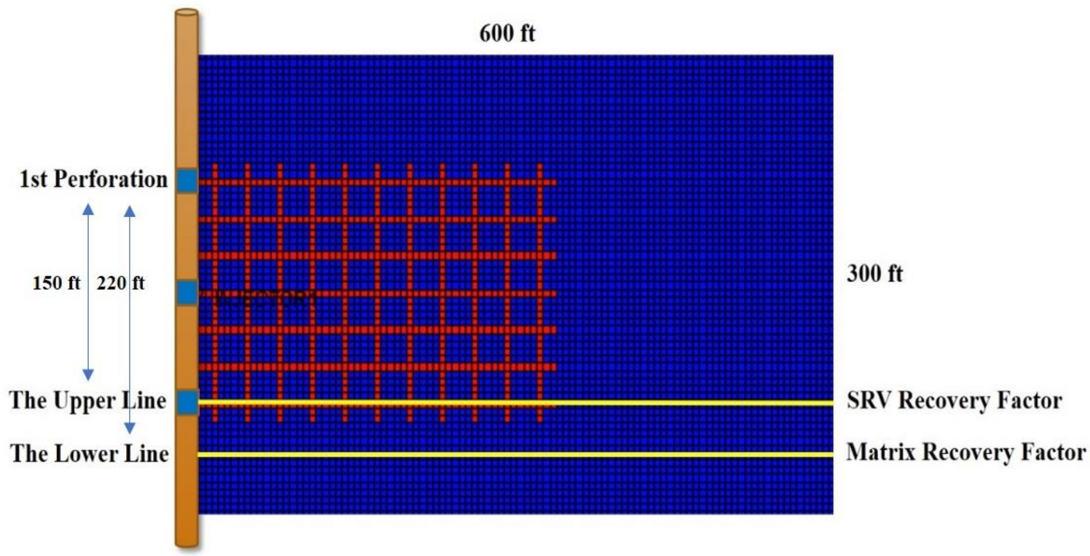

Figure 4-6. Schematic View of the Matrix Depletion Factor and the SRV Depletion Factor

In order to figure out the influences of SRV regions, two yellow lines are selected in Figure 4-6. The upper line crosscuts the artificially fractured regions. Thus, most blocks along the upper line are inside the SRV region. In contrast, blocks along the lower line are in the matrix region. Given this, the depletion factors of blocks along the lower yellow line are the matrix depletion factors. Natural gas can flow from the original matrix blocks to the neighboring blocks and eventually flow to the blocks adjacent to the wellbore. This explains that how the natural gas in the matrix region becomes produced.

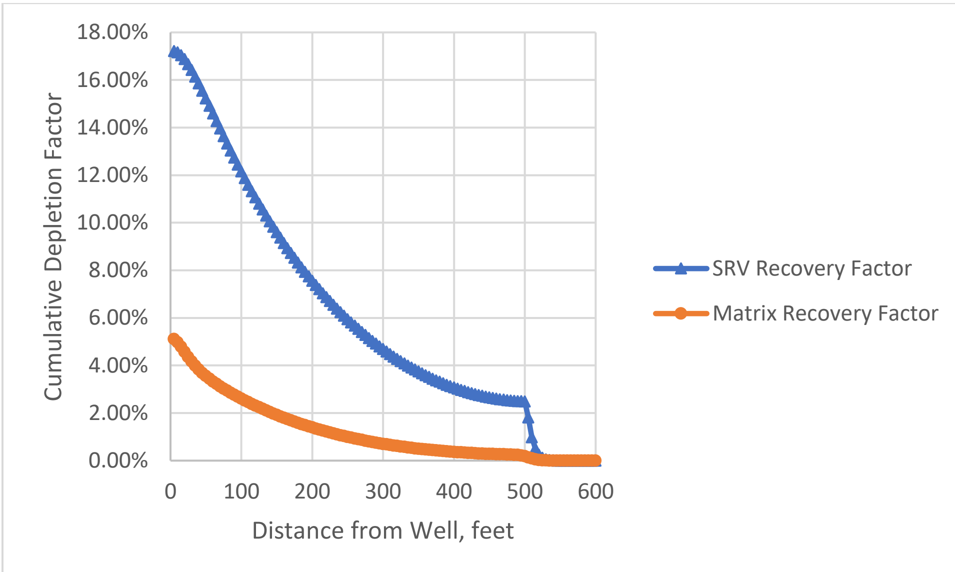

Figure 4-7. SRV and Matrix Cumulative Depletion Factor along the Fracture Direction over 15 Years

When the production time is set to be 15 years, Figure 4-7 shows the cumulative depletion factors of the locations on both yellow lines of Figure 4-6. As can be shown here, the range of the matrix depletion factor is from 0% to 5%. Those low matrix depletion factors indicate that small amount of natural gas is produced from the regions outside the SRV. In contrast, the SRV depletion factor is always higher than the matrix depletion factor across 15 years. Further, low depletion factors in the matrix region mean that most natural gas outside the SRV region is not migratory.

4.2.3 Depletion Factors at Different Times

The well production times are chosen to be one year, five years, ten years and fifteen years. Running the base model and making the volumetric calculations give the natural gas depletion factors at each block. For the blocks having the same distance from the wellbore, the mean depletion factor of those blocks across the wellbore direction is taken as the depletion factor at that distance from the wellbore.

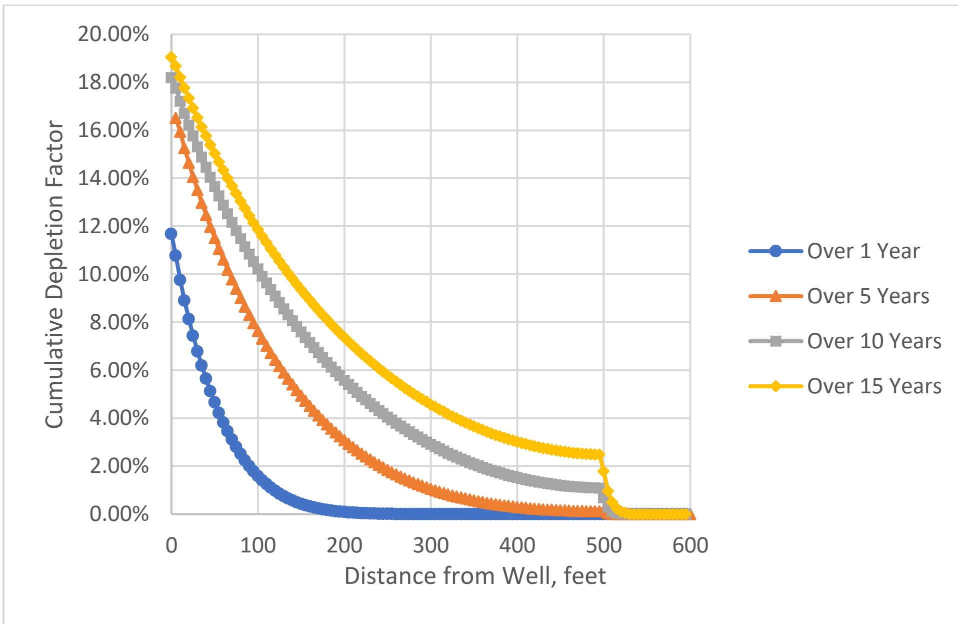

Figure 4-8. Cumulative Gas Depletion Factors along the Fracture Direction across Different Years

Figure 4-8 shows the recovery changes as a function of the distance from wellbore. When the distance from wellbore keeps increasing, the cumulative depletion factor will decrease. Also, the cumulative natural gas production will increase with the production time. However, the cumulative depletion factors of all selected years have a drop at the Stimulated Reservoir Volume boundary whose distance from the wellbore is 500 feet.

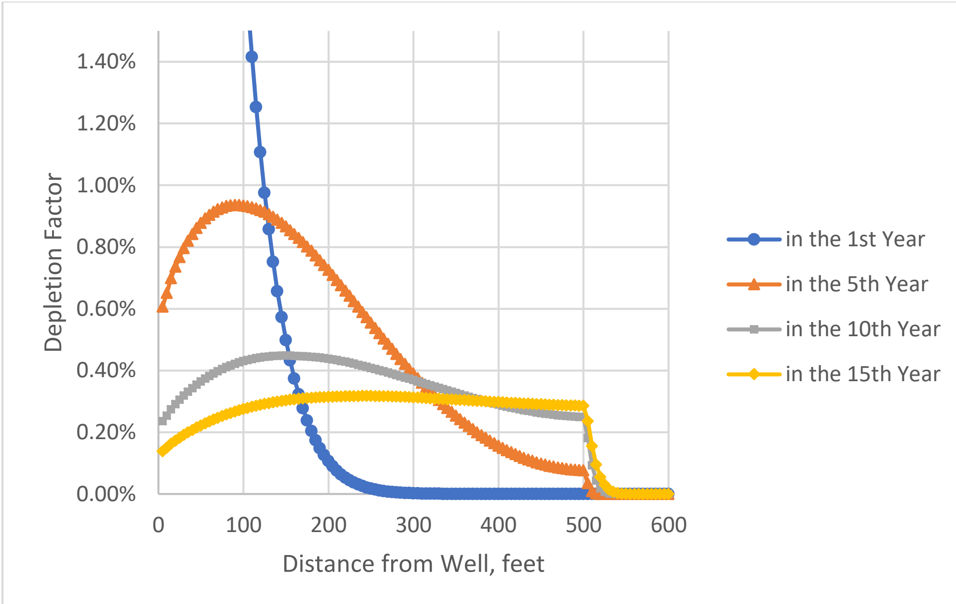

Figure 4-9. Gas Depletion Factor Rate along Fracture Direction in Different Years

Figure 4-9 indicates that when the production time increases, the production in each year will decrease accordingly. For the 1st year, the gas production from locations within 150 feet accounts for 97.7% of the total production. In the first five years, 76.6% of the natural gas production comes from the region within 150 feet from the wellbore. When the production time comes to the 10 years, locations whose distance is less than 150 feet provides 63.3% of the total gas production. In contrast, the production from locations distant from the wellbore increases with the production time. When the time is 15 years, natural gas from all locations inside the SRV region is flowing to the well.

Depletion factor fractional contribution (FC) is the depletion factor at the selected location divided by the total depletion factors in a certain area:

$$FC_i = \frac{DF_i}{\sum_{i=1}^{120} DF_i} \tag{7}$$

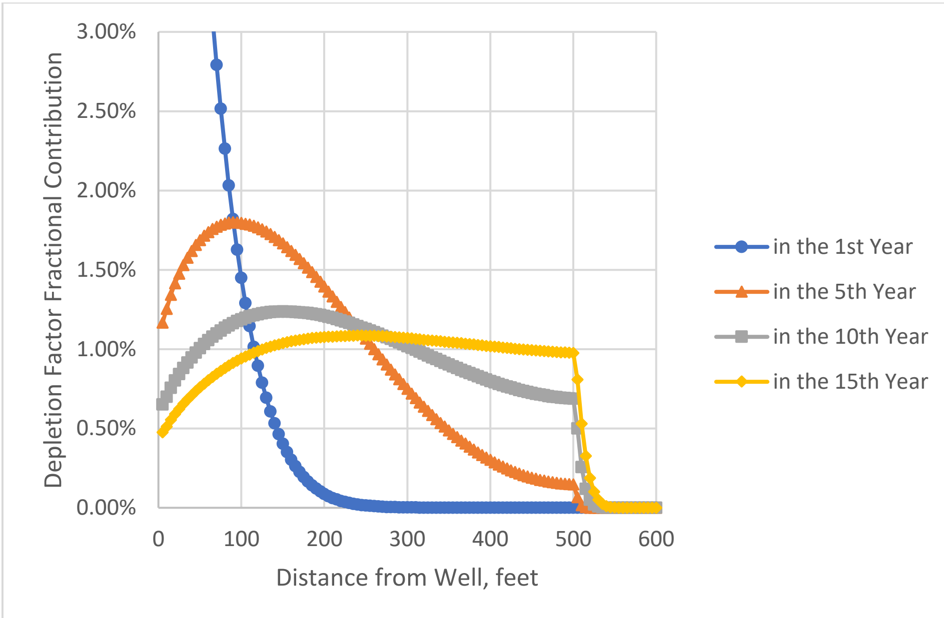

Figure 4-10. Depletion Factor Fractional Contribution along the Fracture

Figure 4-10 shows that the regions within 500 feet from the wellbore account for 99.51% of total natural gas depletion. Compare the depletion factor fractional contribution in different years. As the production time increases, the areas adjacent to the wellbore accounts for lower proportions of the total natural gas recovery and the areas distant from the wellbore will have higher depletion factors.

Another interesting parameter is the cumulative fractional contribution (CFC). The CFC represents the sum of FCs whose distance is smaller than the selected distance:

$$CFC_i = \sum_1^i FC_i \tag{8}$$

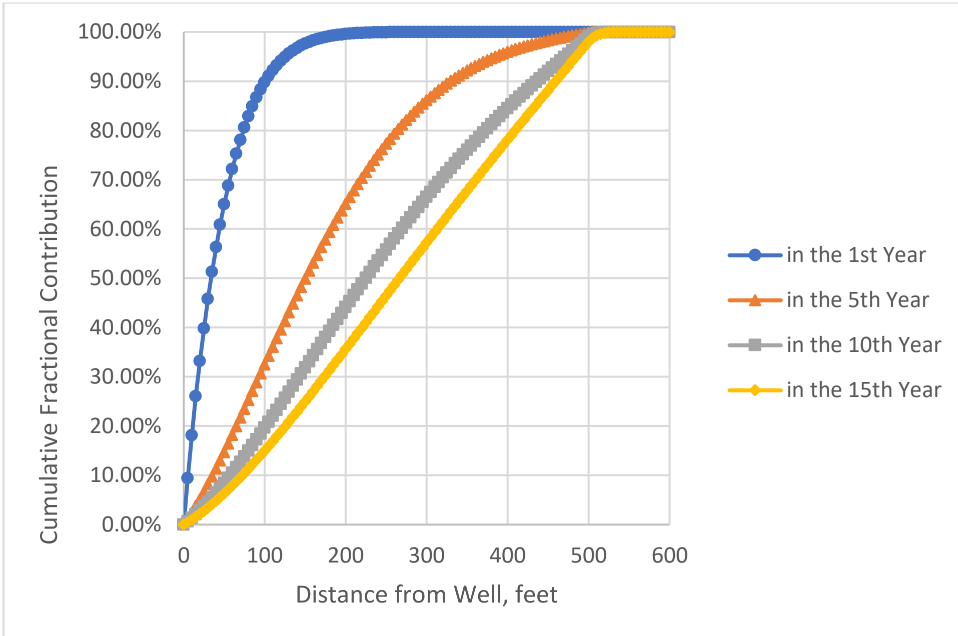

Figure 4-11. Cumulative Fractional Contribution along the Fracture Direction

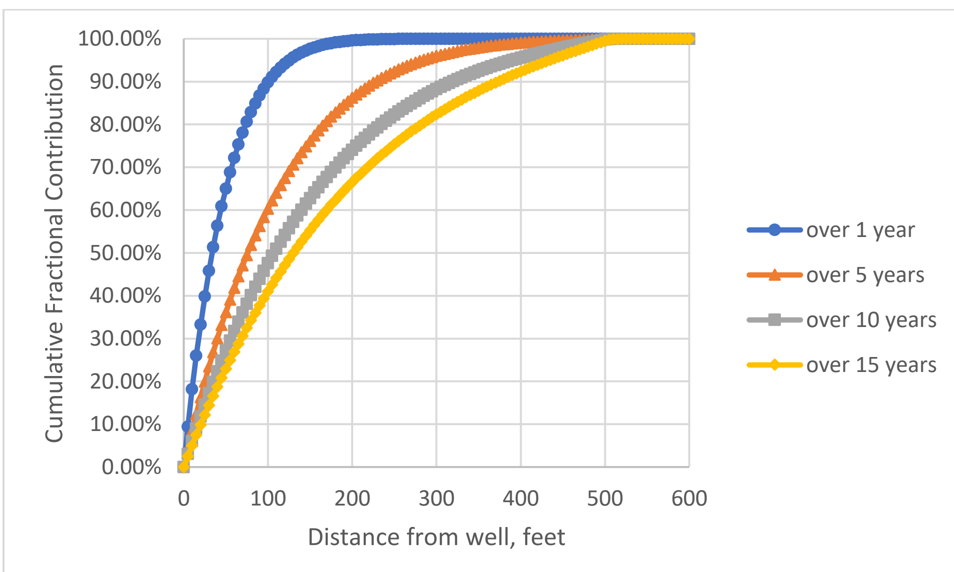

Figure 4-12. Total CFC for the Combination over 15 Years

Figure 4-11 shows that all fractional contribution in the different years become stable when the distance along the fracture propagation direction is equal or greater than 500 feet. The natural gas flowing from the locations outside the SRV region accounts for nearly 0% of the total gas production. The total CFC (Figure 4-12) indicates that wells having shorter production time tend to produce the natural gas from closer areas. When the production time increases, more gas will be produced from distant locations. Additionally, natural gas is mainly produced from the SRV region. This case is not only suitable for wells having short production time but also for wells having longer production time.

Chapter 5

Sensitivity Study

Estimating the amount of natural gas that is removed from a specific plot of land is complex. Many factors can influence the natural gas depletion factor outcomes. In this chapter, I perform a set of sensitivity studies to quantify the relative impact of uncertainty in different problem parameters.

Table 5-1. Values of Parameters in the Sensitivity study

Parameters	Values
Natural Fracture Spacing, feet	3×1; 20×10; 200×100
Permeability of Matrix, md	10^{-4}; 10^{-2}
Conductivity of Hydraulic Fractures, md-ft	0.1; 1; 10; 100; 1,000
Bottom-hole Pressure, psi	300; 2,000
Pore Pressure Gradient, psi/ft	0.4; 0.6

Each of the selected input parameters have a set of plausible values. In this analysis, I modify each input parameter, one at a time, and compare the change in the model outcomes. The sensitivity analysis informs how the input variable change can influence the simulation results.

The parameters explored here are natural fracture spacing, permeability of natural fractures, conductivity of hydraulic fractures, bottom-hole pressure and pore pressure. Table 5-1 lists the range of values of these parameters that can be found in the literature.

Table 5-2. Base Case for Selected Parameters in the Sensitivity study

Parameters	Base Model Value
Natural Fracture Spacing, feet	3×1
Permeability of Matrix, md	10^{-4}
Conductivity of Hydraulic Fractures, md-ft	4
Bottom-hole Pressure, psi	2,500
Pore Pressure Gradient, psi/ft	0.4

5.1 Effect of Natural Fracture Spacing

The two fracture sets in the Marcellus shale are not evenly spaced. In Figure 2-1, the fracture set J2 running to the north-northwest direction is more widely spaced than the fracture set J1 running to the east-northeast direction (Engelder et al., 2009). From the viewpoint of geomechanics, the contemporary tectonics stress field in the Appalachian basin favors the horizontal drilling directed to the NNW or SSE. Thus, the hydraulic fractures conducted by producers are designed to reopen and efficiently drain the more narrowly formed J1 joint sets. In our model, the fracture spacing in the fracture propagation direction is greater than the fracture spacing along the wellbore direction.

To simulate the effect of natural fracture spacing on the depletion factor in the Marcellus shale, three natural fracture spacing sets are chosen. They are 3 feet × 1 feet, 20 feet × 10 feet and 200 feet × 100 feet. Different natural fracture spacings are examined while other parameters are kept unchanged in the simulation.

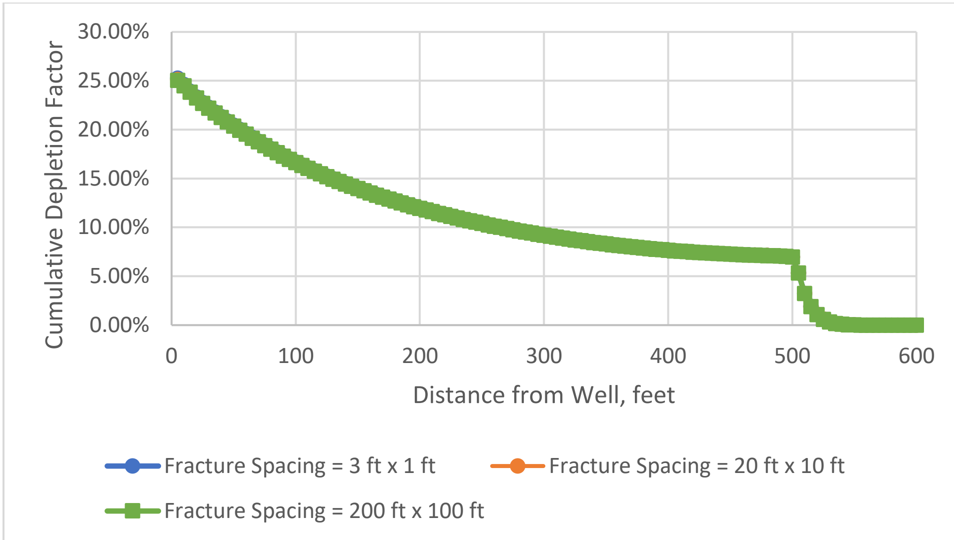

Figure 5-1. Cumulative Depletion Factors along the Fracture Direction over 15 Years for Different Natural Fracture Spacings

Figure 5-1 shows the cumulative depletion factor over 15 years for different natural fracture spacings. From Figure 5-1, when the natural fracture spacing increases from 3 feet × 1 feet to 200 feet × 100 feet, there is 0.21% decrease of the cumulative depletion factor. Smaller natural fracture spacing means that natural fracture systems have a higher fracture density. Thus, the cumulative depletion factor increases with the decreasing natural fracture spacing. However, the natural fracture spacing is not a significant factor, because the low matrix permeability prevents more natural gas from getting extracted.

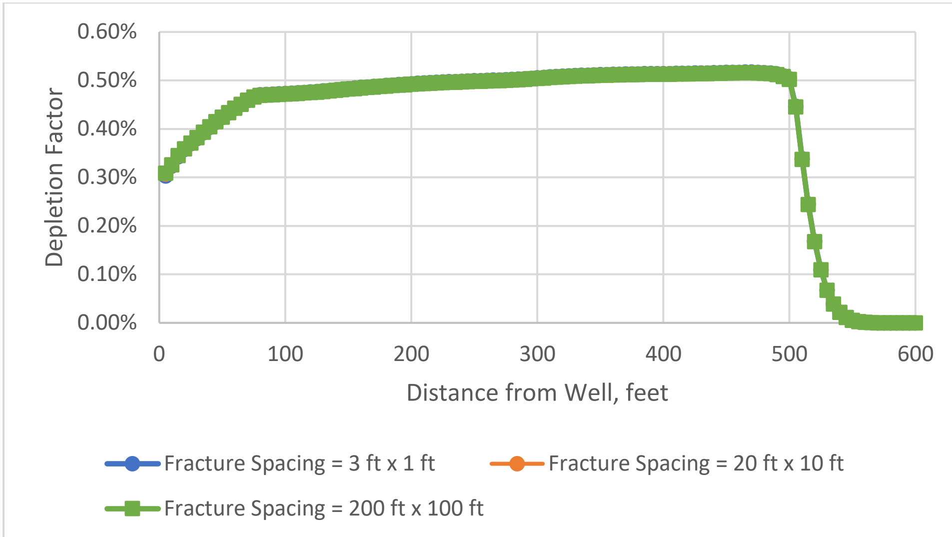

Figure 5-2. Depletion Factor Rates along the Fracture Direction in the 15th Year for Different Natural Fracture Spacings

Figure 5-2 shows the depletion factor rate in the 15th year for the three sets of natural fracture spacings. The depletion factor rate in the 15th year is approximately unchanged when the natural fracture spacing increases. It is true that the natural fractures and the hydraulic fractures work together to drain the natural gas. However, this sensitivity analysis only focuses on the impacts of the natural fracture spacing. The hydraulic fracture spacings are not adjusted depending on the natural fracture spacings.

5.2 Effect of Matrix Permeability

In order to study the effects of matrix permeability, two sets of matrix permeability are used to make comparisons. The first matrix permeability is 0.0001 md and the second matrix permeability is 0.01 md.

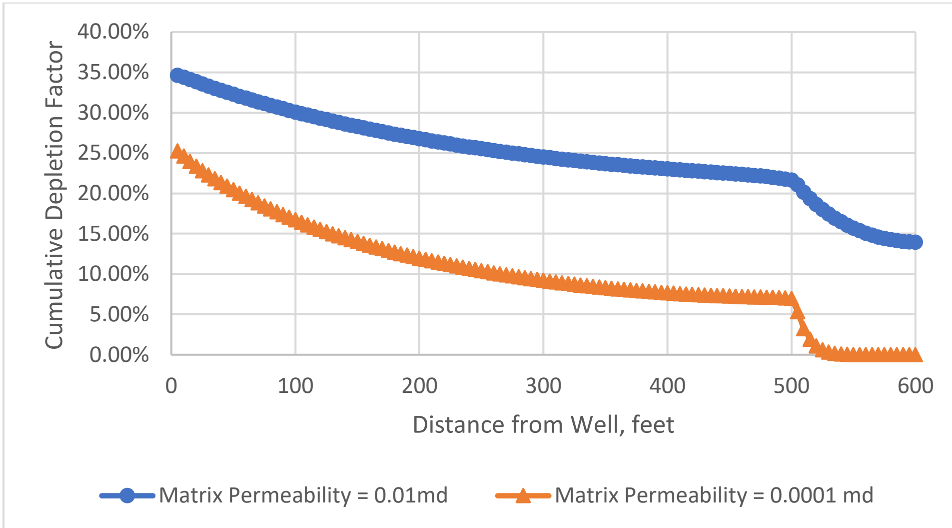

Figure 5-3. Cumulative Depletion Factors along the Fracture Direction over 15 Years for Different Matrix Permeabilities

The comparison of the cumulative depletion factors for different matrix permeabilities shows that the change of matrix permeability has a significant effect on the simulation result. Changing the matrix permeability from 0.0001 md to 0.01 md increases the cumulative gas depletion factor by 9.35%.

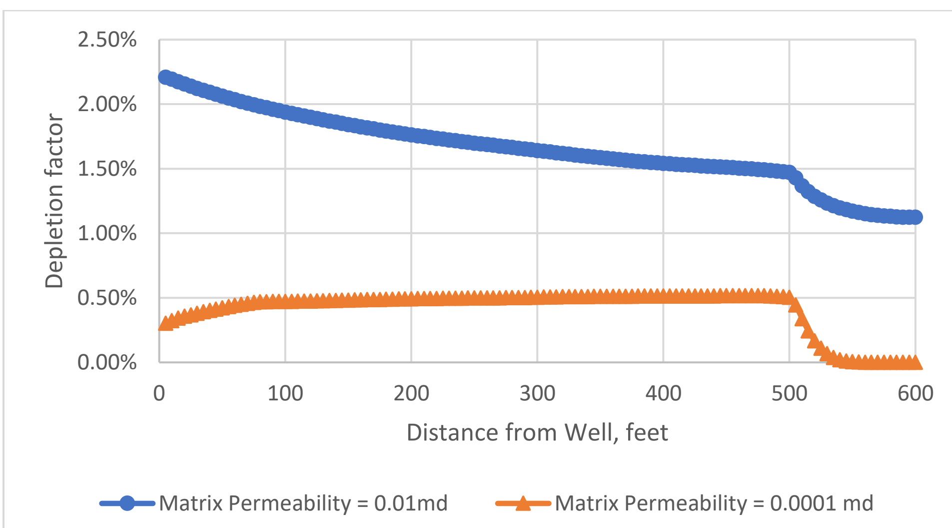

Figure 5-4. Depletion Factor Rates along the Fracture Direction in the 15th Year for Different Matrix Permeabilities

Figure 5-4 shows that the depletion factor rate in the 15th year is increased by 1.91% when the matrix permeability is increased to 0.01 md. Even though there is still a drop of depletion factor at the boundary of the SRV region, the depletion factor rate in the 15th year at the SRV boundary is increased by 1% when changing the matrix permeability from 0.0001 md to 0.01 md.

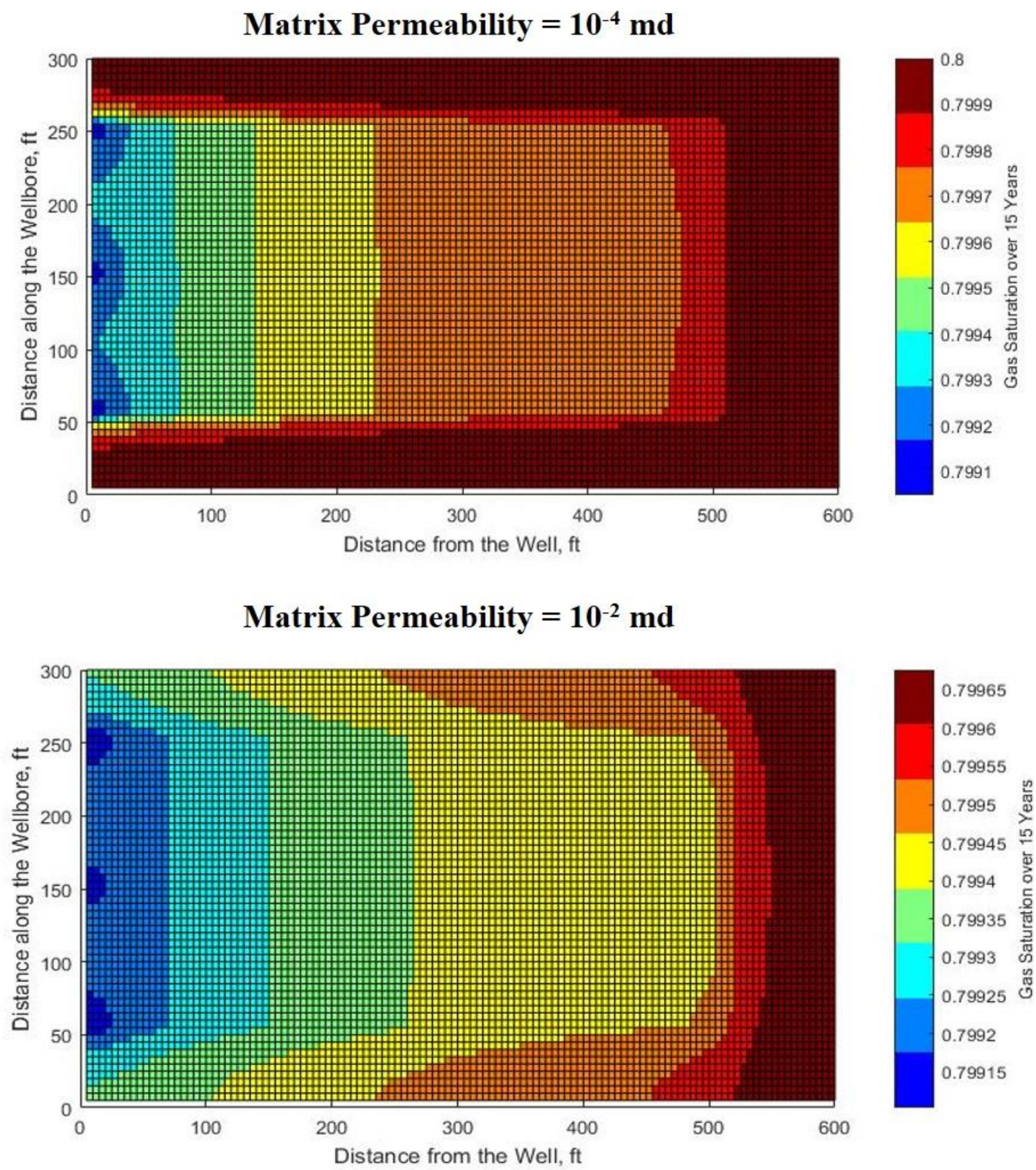

Figure 5-5 Gas Saturation Distribution after 15 Years for Different Matrix Permeabilities

The increase of matrix permeability improves the flow capability from high-pressure areas to low-pressure areas. Additionally, from the natural gas distribution plot in Figure 5-5, higher matrix permeability makes all the gas in the modeled reservoir migratory. Not only the depletion factors inside SRV region but also the depletion factors in the matrix region are greater than zero.

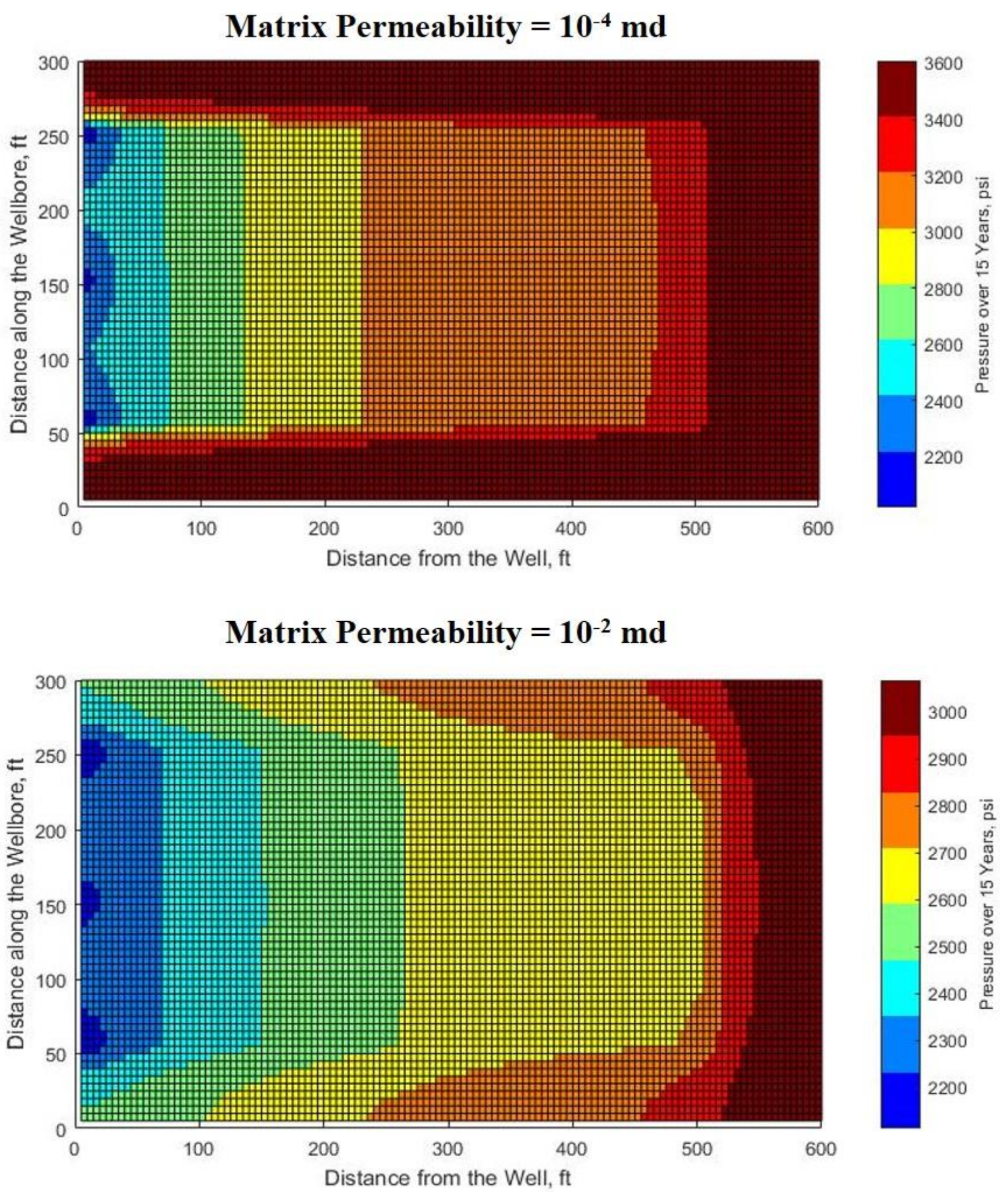

Figure 5-6. Pressure Distribution after 15 Years for Different Matrix Permeabilities

Figure 5-6 shows the pressure distribution after 15 years associated with different matrix permeabilities. The dark blue regions represent the bottom-hole pressure and the dark red areas represent the initial pressure of the reservoir. For the higher matrix permeability case, more locations have pressure drops and the natural gas is drained more effectively.

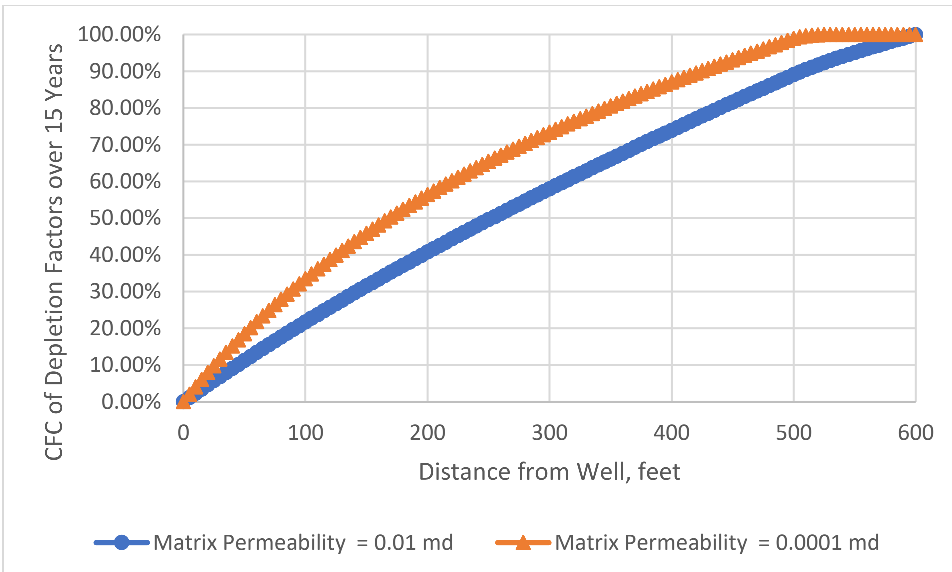

Figure 5-7. Cumulative Fractional Contribution of Depletion factor for Different Matrix Permeability

Figure 5-7 shows the cumulative fractional contribution of DF for different matrix permeabilities. The red line represents the CFC for a matrix permeability of 0.0001 md, while the blue line shows the CFC curve for a matrix permeability of 0.01 md. When the matrix permeability is low, most natural gas is produced from the locations within 500 feet. In contrast, when the matrix permeability is increased to 0.01 md, the natural gas from locations from 500 feet to 600 feet accounts for 10% of the total gas production. Thus, increasing matrix permeability makes the natural gas drainage area extend to more distant locations.

5.3 Effect of Hydraulic Fracture Conductivity

Conductivity of the hydraulic fracture measures the product between the hydraulic fracture width and the hydraulic fracture permeability. Hydraulic fractures are generated to connect the gas well to the natural fracture network (Engelder et al., 2009). Thus, a higher conductivity means an easier channel for the natural gas to flow from the natural fractures to the gas well. In the sensitivity study on the fracture conductivity, the hydraulic fracture conductivities are chosen to be 0.1 md-ft, 1 md-ft, 10 md-ft, 100 md-ft and 1,000 md-ft.

If a laminar flow moves through a fracture with parallel planar surfaces, the hydraulic conductivity is calculated by:

$$K_f = \frac{(2b)^2 \rho g}{12\mu} \qquad (9)$$

where K_f is the hydraulic conductivity, b is the aperture half width, ρ is the fluid density, g is the acceleration of gravity and μ is the flow viscosity (Witherspoon et al., 1980). When the flow is isothermal and steady, the Darcy's law can be used to calculate the flow rate using:

$$\frac{q}{\Delta h} = C(2b)^3 \qquad (10)$$

where q is the flow rate, Δh is the hydraulic head drop and C is a constant. C is given depending on the flow type. If the case is the straight flow, C is expressed as:

$$C = \left(\frac{w}{\mathrm{L}}\right)\left(\frac{\rho g}{12\mu}\right) \qquad (11)$$

where w is the width of fracture and L is the length of fracture. In contrast to the straight flow, the radial flow case uses C as:

$$C = \left(\frac{2\pi}{\ln(\frac{r_e}{r_w})}\right)\left(\frac{\rho g}{12\mu}\right) \qquad (12)$$

where r_e is the outer radius and r_w is the wellbore radius. Equation (10) is commonly referred to as the cubic law to characterize the flow in fractures (Witherspoon et al., 1980).

The hydraulic fracture conductivity is the product of fracture aperture width times the fracture permeability. For laminar flow, the fracture conductivity can be developed by Darcy's law and written as a function of hydraulic conductivity K_f.

In order to make the selected values of hydraulic fracture conductivities reliable, the cubic law characterizing the laminar flow in a fracture should be used. From the cubic law equations, the hydraulic fracture conductivities should scale to the cubic power of the fracture aperture width.

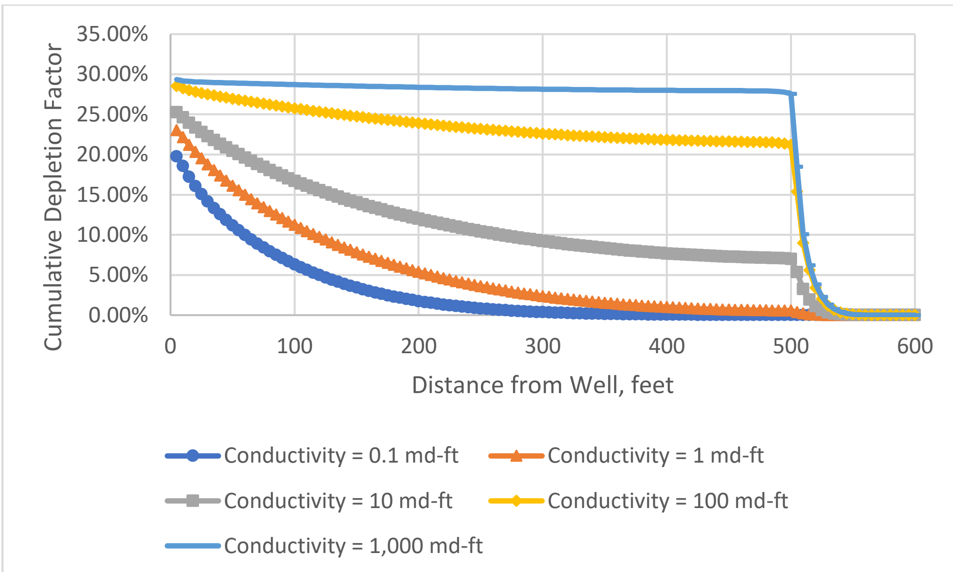

Figure 5-8. Cumulative Depletion Factors along the Fracture Direction over 15 Years for Different Hydraulic Fracture Conductivities

As can be shown in Figure 5-8, increasing the hydraulic fracture conductivities results in a significant rise of the cumulative depletion factors. The simulation with 1,000 md-ft hydraulic fracture conductivity has the highest cumulative gas depletion factor. Changing the conductivity from 10 md-ft to 100 md-ft increases the cumulative depletion factor by 12.65%. The reason is that natural gas flows more easily from the natural fracture network to the wellbore when there is an increase of the hydraulic fracture conductivity.

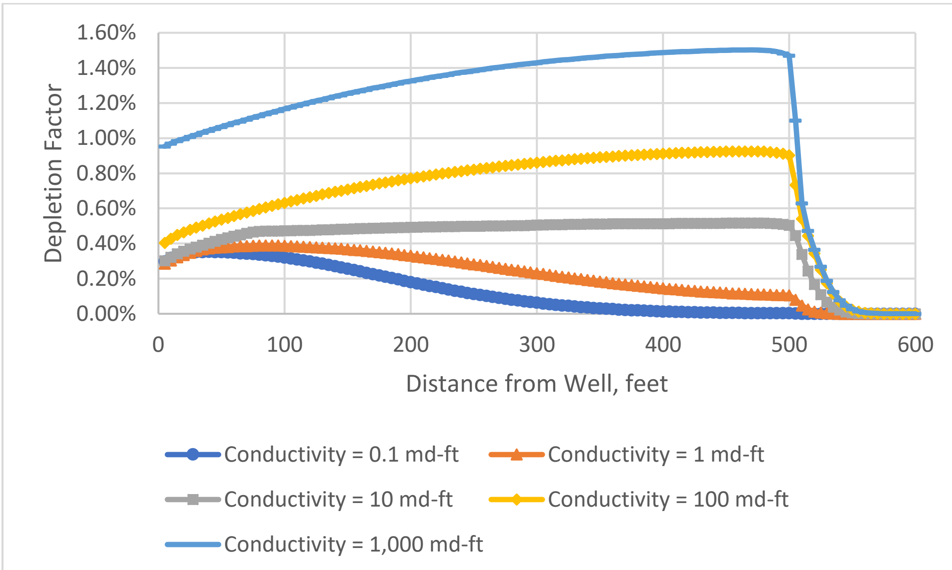

Figure 5-9. Depletion Factor Rates along the Fracture Direction in the 15th Year for Different Hydraulic Fracture Conductivities

Figure 5-9 shows that depletion factor rate associated with the higher conductivity is greater than the recovery rate associated with the lower conductivity. In addition, the gas depletion amount in the locations with a greater distance from the well increases significantly with the hydraulic fracture conductivity. At the distance of 300 feet, changing the conductivity from 10 md-ft to 100 md-ft increases the depletion factor rate by 0.36%. In contrast, the depletion factor rate is only increased by 0.11% when the location has the distance of 50 feet from the well.

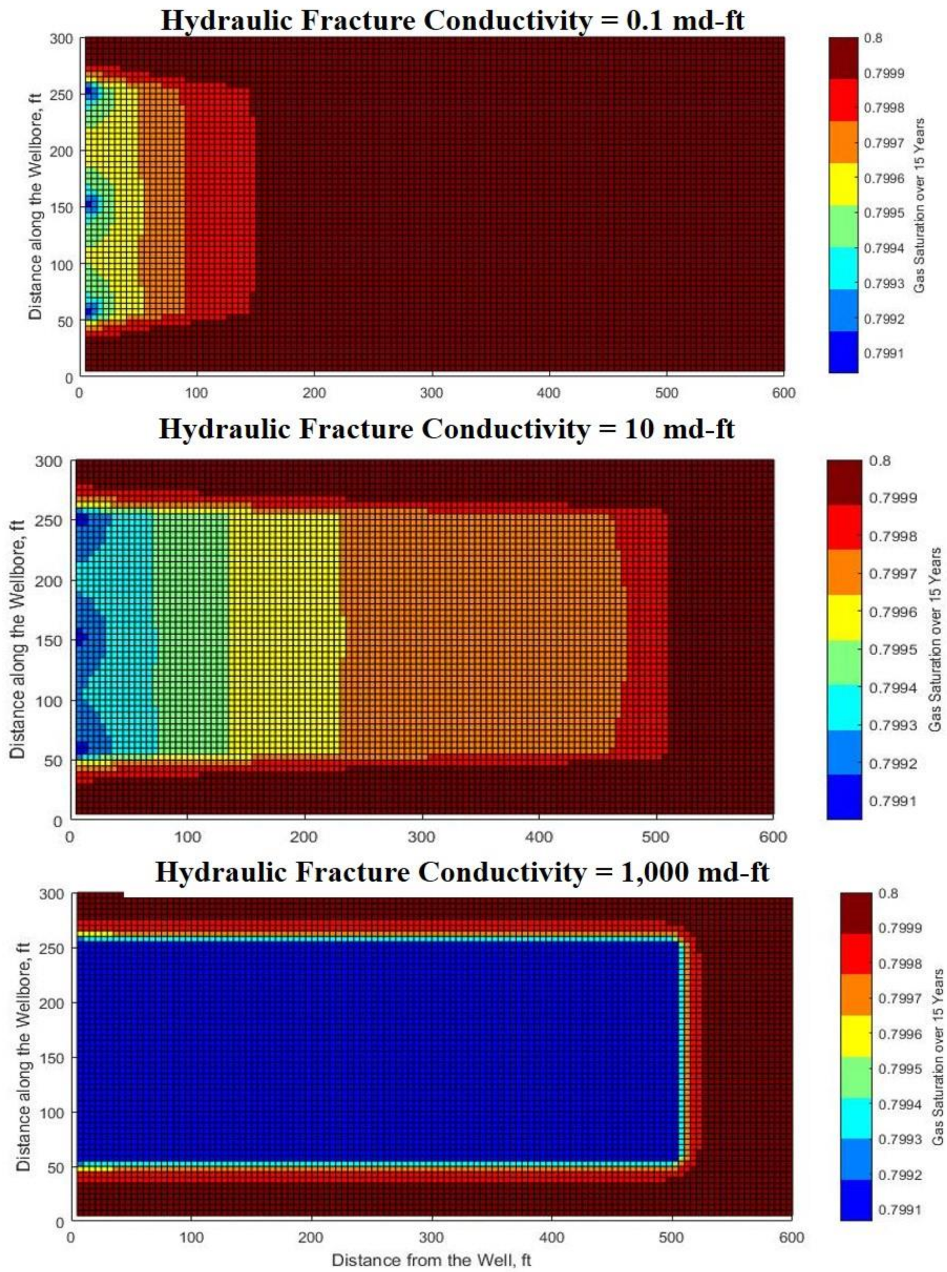

Figure 5-10. Gas Saturation Distribution after 15 Years for Different Fracture Conductivities

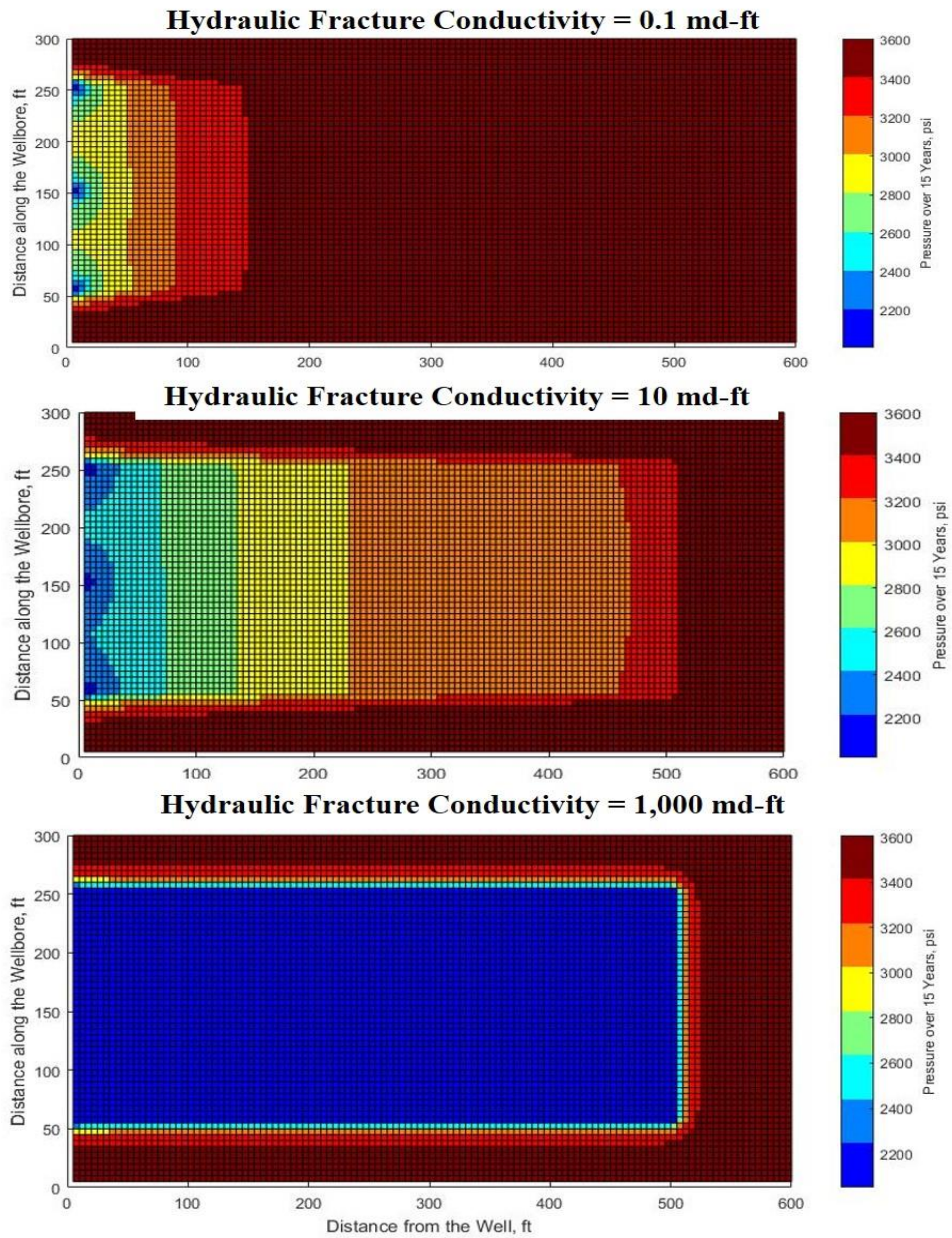

Figure 5-11. Pressure Distribution after 15 Years for Different Fracture Conductivities

Figure 5-11 shows the pressure distribution after 15 years for different hydraulic fracture conductivities. The dark blue regions represent the bottom-hole pressure, while the dark red areas represent the initial pressure of the reservoir. For the conductivity of 1,000 md-ft case, nearly every location inside the SRV has the pressure close to the bottom-hole pressure. The natural gas becomes drained effectively in this case. In contrast to the SRV region, quite a lot of natural gas still keeps trapped in the matrix region.

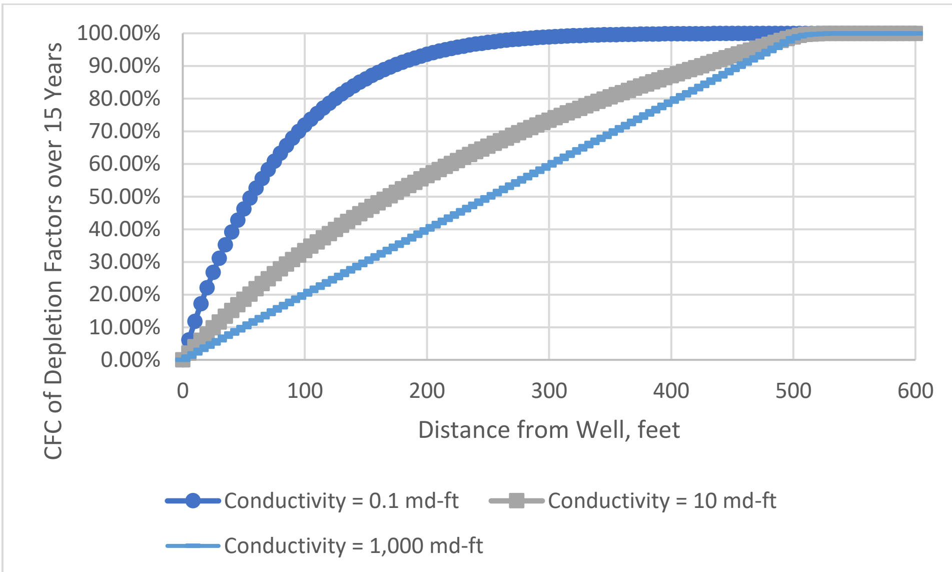

Figure 5-12. Cumulative Fractional Contribution of Depletion Factor for Different Fracture Conductivities

Figure 5-12 shows the cumulative fractional contribution for different fracture conductivities. When the fracture conductivity is 0.1 md-ft, most natural gas is produced from locations within 300 feet. In contrast, when the conductivity is changed to 10 md-ft, the natural gas from locations within 300 feet accounts for 74.18% of the total gas production. However, from Figure 5-12, increasing the conductivity from 10 md-ft to 1,000 md-ft almost does not change the gas drainage area in the model. This result shows that the hydraulic fracture conductivities in the sensitivity analysis are likely not appropriately selected. The hydraulic fracture conductivity samples should scale to the cubic power of the fracture aperture width.

5.4 Effect of Pore Pressure

Pore pressure has a great influence on formation effective pressures. This model expects the reservoir to be normally pressured. Thus, the formation pressure is the product of formation depth times the pore pressure gradient. During the natural gas production process, the difference between the formation pressure and the bottom-hole pressure determines the gas flow rate and the cumulative production. In our sensitivity study, the pore pressure gradients are set to be 0.4 psi/ft and 0.6 psi/ft.

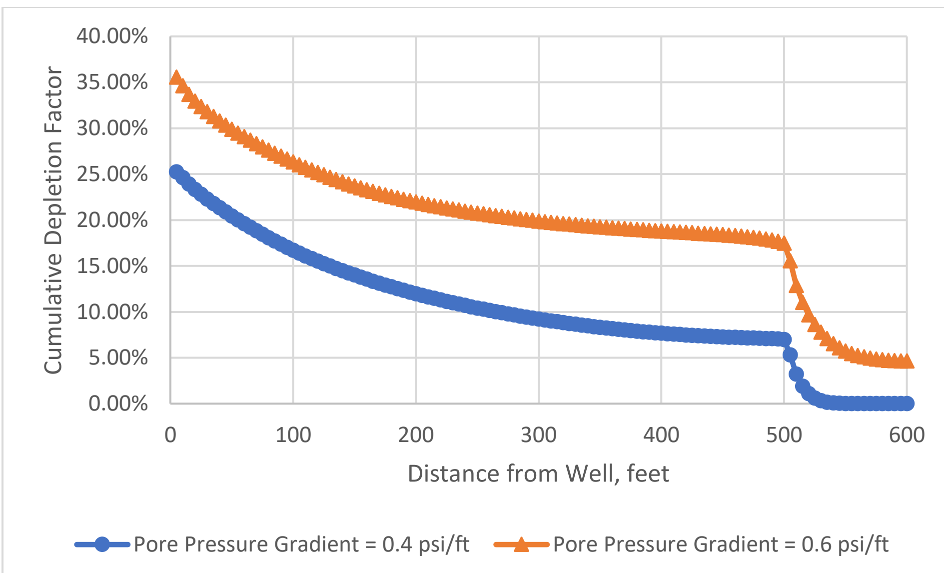

Figure 5-13. Cumulative Depletion Factors along the Fracture Direction over 15 Years for Different Pore Pressure Gradients

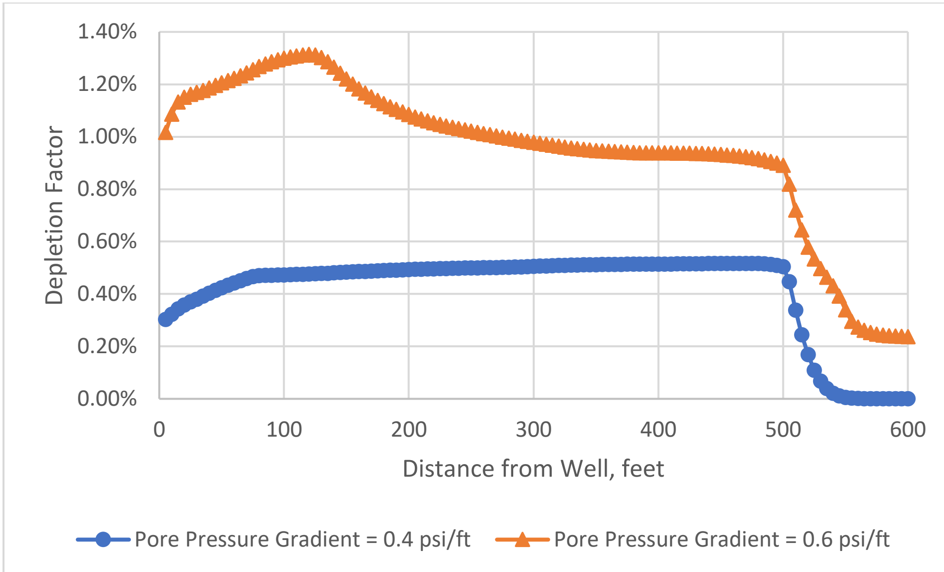

Figure 5-14. Depletion Factor Rates along the Fracture Direction in the 15th Year for Different Pore Pressure Gradients

Figure 5-13 and Figure 5-14 show that the cumulative gas depletion factor and the depletion factor rate associated with two different pore pressure gradients. Increasing the pore pressure gradient from 0.4 psi/ft to 0.6 psi/ft increases the cumulative depletion factor by 15%. In Figure 5-14, the curve of 0.6 psi/ft pore pressure gradient has a strange behavior from zero to 200 feet. A sensitivity study is needed to adjust the grid size and to examine the corresponding behaviors of the curve.

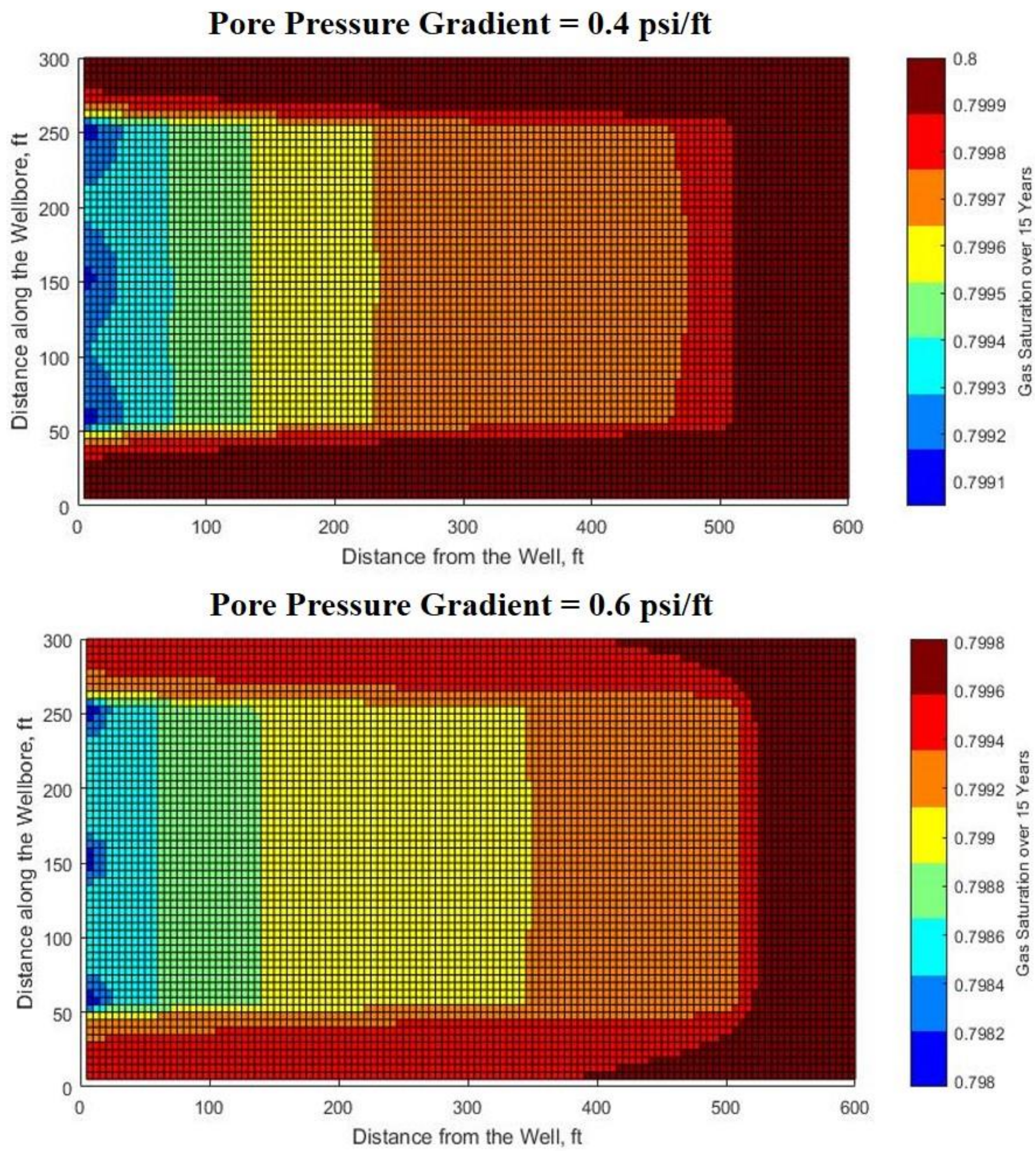

Figure 5-15. Gas Saturation Distribution after 15 Years for Different Pore Pressures

Additionally, from the gas saturation distribution information in Figure 5-15, the increase of the pore pressure results in the rise of depletion factors at all locations in the modeled reservoir. Formation pressure increases with the pore pressure gradient. Thus, when the bottom-hole pressure is kept constant, the increase of the difference between the formation pressure and the bottom-hole pressure results in the gas flow with a greater flowing capability.

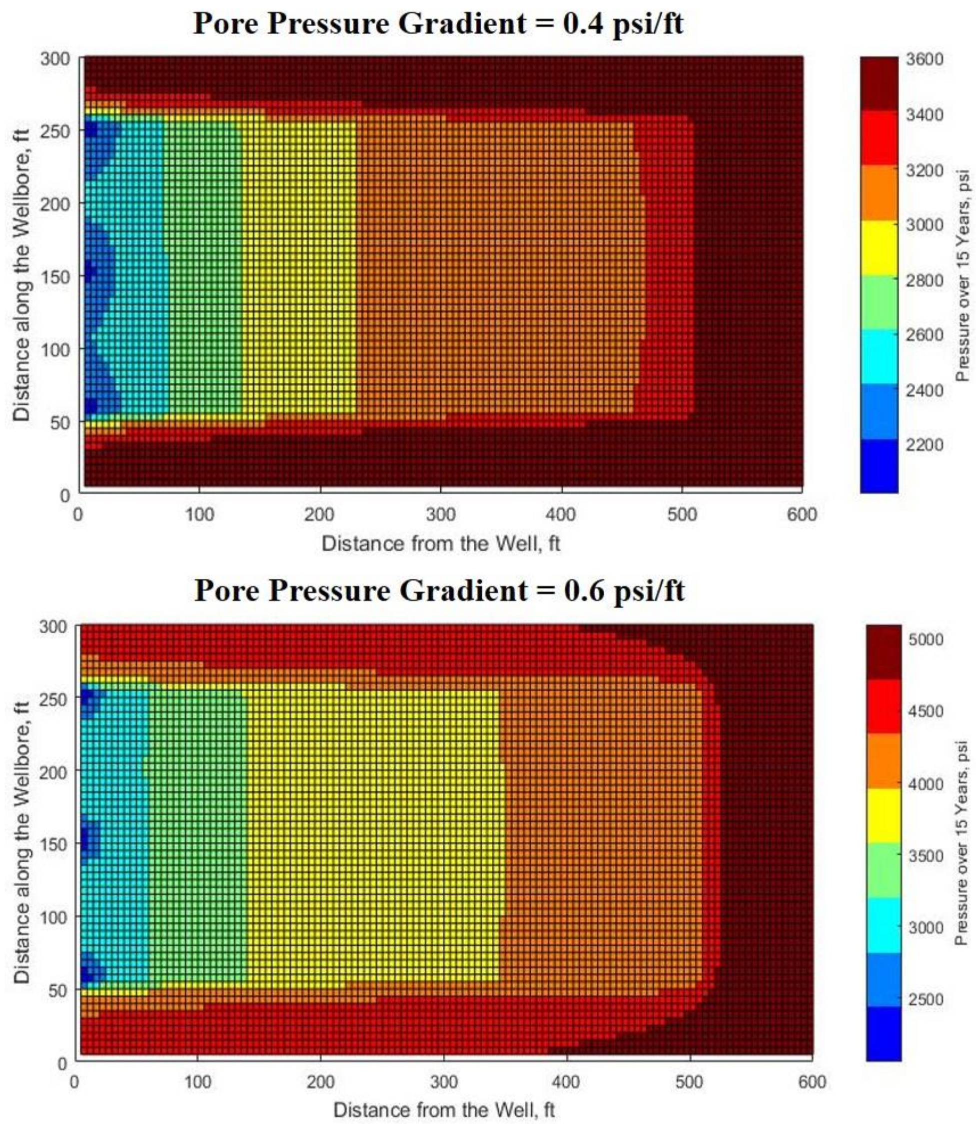

Figure 5-16. Pressure Distribution after 15 Years for Different Pore Pressures

Figure 5-16 shows the pressure distribution for different pore pressure conditions. The dark red regions represent the initial pressure of the reservoir and the dark blue areas represent the bottom-hole pressure. For the higher pore pressure case in Figure 5-16, more locations have pressure drops and the natural gas is drained more effectively.

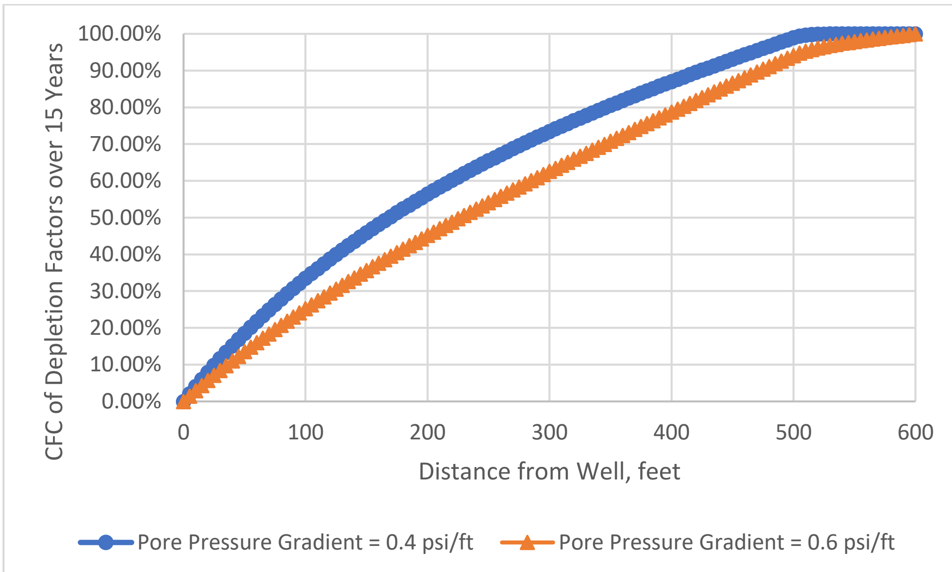

Figure 5-17. Cumulative Fractional Contribution of Depletion Factor for Different Pore Pressures

Figure 5-17 shows the cumulative fractional contribution associated with different pore pressures. When the pore pressure gradient is increased from 0.4 psi/ft to 0.6 psi/ft, natural gas starts to flow from the locations with the distance greater than 500 feet. Thus, increasing the pore pressure enlarges the natural gas drainage area along the fracture propagation direction.

5.5 Effect of Bottom-hole Pressure

As we have discussed in the pore pressure section, bottom-hole pressure also has a significant influence on the gas production. The depletion factor rate and the cumulative depletion factor change with the difference between the formation pressure and the bottom-hole pressure. The bottom-hole pressure is required to be lower than the reservoir pressure. Thus, gas will flow from high-pressure locations to the producer's well. The low bottom-hole pressure in our sensitivity study is 300 psi and the high bottom-hole pressure is 2,000 psi.

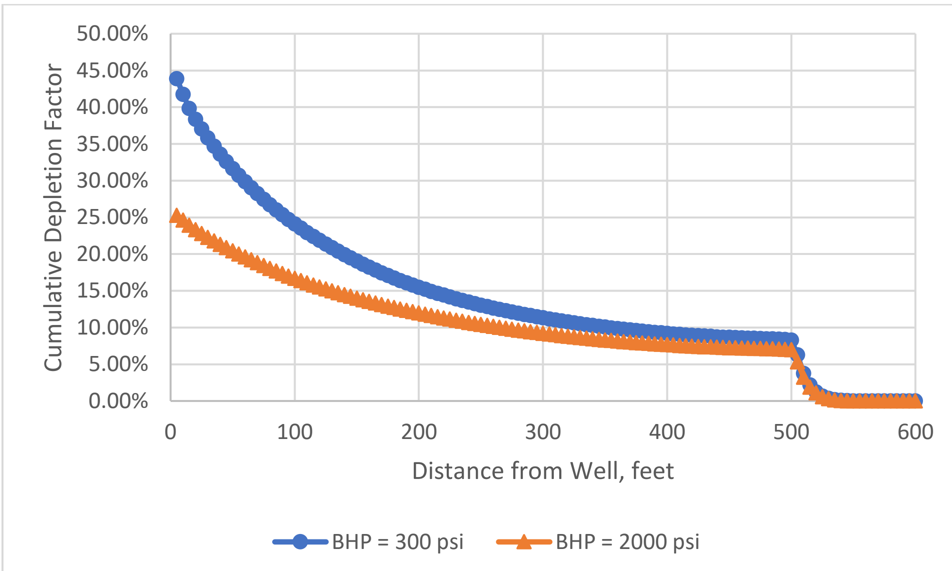

Figure 5-18. Cumulative Depletion Factors along the Fracture Direction over 15 Years for Different Bottom-hole Pressures

Figure 5-18 and Figure 5-19 show that the cumulative gas depletion factor and the depletion factor rate associated with two different bottom-hole pressures. The lower bottom-hole pressure case increases the cumulative depletion factor by 7.83%. Lower bottom-hole pressure increases the pressure difference between the gas well and the reservoir. Thus, natural gas flow rate increases and more gas become depleted. Additionally, from Figure 5-18, the big difference of depletion factors associated with two bottom-hole pressures within 100 feet indicates that adjusting the bottom-hole pressure only affects the depletion factors near the wellbore.

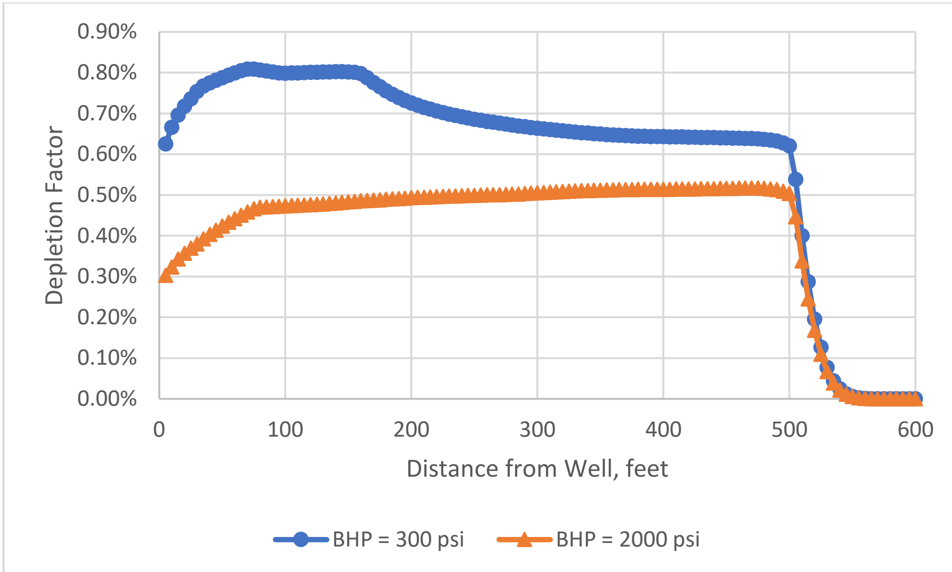

Figure 5-19. Depletion Factor Rates along the Fracture Direction in the 15th Year for Different Bottom-hole Pressures

From zero to 200 feet, the depletion factor curve of 300 psi bottom-hole pressure has an interesting behavior. In order to understand this behavior, the time step and the grid size need to be adjusted and the corresponding curve shapes can be studied.

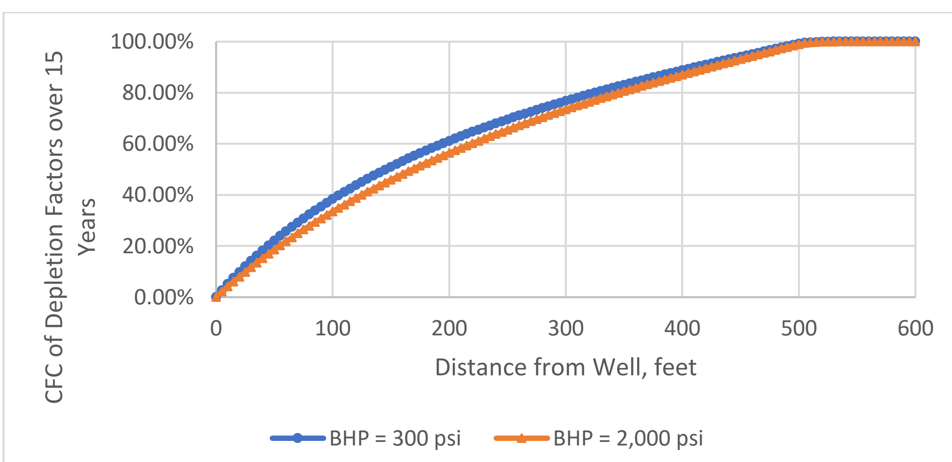

Figure 5-20. Cumulative Fractional Contribution of Depletion Factor for Different Bottom-hole Pressures

Figure 5-20 shows cumulative fractional contribution for two different bottom-hole pressures. For the case of 300 psi, the locations closer to the wellbore have a higher depletion factor increase when compared with the locations with a greater distance from the well. The reason is that bottom-hole pressure only influences the pressure difference adjacent to the well. Changing the bottom-hole pressure does not interfere with the gas flow distant from the wellbore.

Chapter 6

Gas Prediction from Landowner's Area

In our petroleum engineering analysis, three typical lands are selected for the simulations. Area I is the land close to the wellbore and upon which is the SRV region, Area II represents the land adjacent to the wellbore while out of the SRV region and Area III is the land distant from the wellbore and the SRV region.

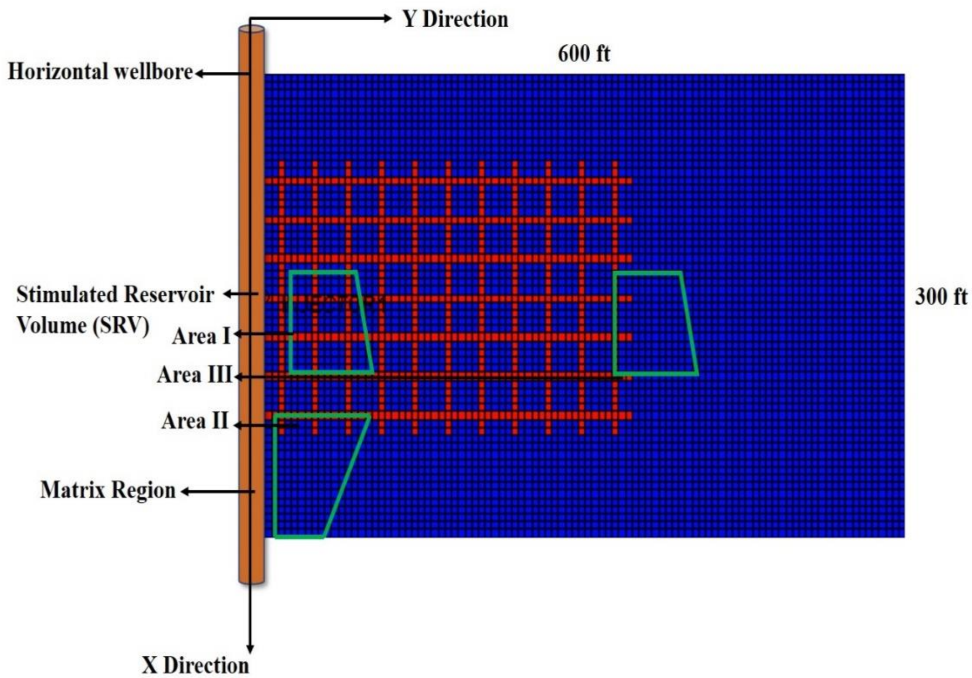

Figure 6-1. Schematic View of the Landowners' Areas

As can be shown in Figure 6-1, a cartesian coordinate system in built in the reservoir. X direction is the wellbore direction while the Y direction is the artificial fracture propagation direction. Assume a landowner has an area described by dimension (x1, y1), (x1, y2), (x2, y1), (x2, y3), with x1<x2, y1<y2, y3 (there is no relationship between y2 and y3).

The red region representing the stimulated reservoir volume (SRV) is under the area I. The artificial fractures do not cross the shale formations below the area II and the area III. In addition, the area II is closer to the wellbore than the other two plots of land. The simulation outcomes are the natural gas migration quantity from these three different types of land.

Table 6-1. Dimensions of Landowner Area I, Area II and Area III

Dimensions	Area I	Area II	Area III
x1, ft	150	240	150
x2, ft	230	300	230
y1, ft	20	10	500
y2, ft	50	70	530
y3, ft	60	45	540

Table 6-1 shows the dimensions of three selected lands: Area I, Area II and Area III. Natural gas that reside under these three lands are likely to flow from the original locations to the wellbore and become extracted at the surface. Chapter 6 measures the trespassed gas from these plots of land and calculates the uncertainty of our estimates. Later, the economic impacts from the trespass rule are examined.

6.1 Samples from Uniform Distribution

Estimation of the extracted shale gas from some specific areas is difficult because of the complex flow in unconventional reservoirs. The formation geology, engineering parameters and operating conditions change with the time, which means that our prediction always has uncertainties.

Change the selected parameters and input those parameters into the model. The next step is to run the simulator for enough times and calculate the coefficient variation of the depletion factors at each location. The heat map of coefficient variation presents the relationship between the uncertainty and the locations of the landowner's area.

Table 6-2. Ranges of Input Parameters in the Uncertainty Calculation

Parameters	Matrix permeability, md	Hydraulic Fracture Conductivity, md-ft	Bottom-hole Pressure, psi	Pore Pressure Gradient, psi/ft
Range	0.0001 – 0.01	0.1 – 1,000	300 – 2,000	0.4 – 0.6
Citation	(Cipolla et al., 2009)	(Cipolla et al., 2008)	(Cipolla et al., 2009)	(Cipolla et al., 2009)

For the uncertainty analysis, each simulation has a new set of four parameters. They are matrix permeability, pore pressure, hydraulic fracture conductivity and bottom-hole pressure.

Many studies in the literature discuss the ranges of selected parameters. In order to study the effects of gas desorption, matrix permeability of 0.0001 md, pore pressure gradient of 0.54 psi/ft and flowing bottom-hole pressure of 1,000 psi are used in Barnett shale reservoir simulations (Cipolla et al., 2009). The matrix permeability of 0.0005 md, bottom-hole pressure of 500 psi and pore pressure gradient of 0.55 psi/ft are the generic Marcellus Shale properties to study the impacts of fracture permeability on the production (Cipolla et al., 2009). For the research on the complex fracture in Barnett shale, the hydraulic fracture conductivities are set to be 0.5 md-ft, 3.3 md-ft, 500 md-ft and 750 md-ft (Cipolla et al., 2008). However, parameters from these references are not for a specific asset.

Table 6-2 shows the ranges of the four selected parameters. From the published article on the shale reservoir simulations, all the numbers within the ranges are equally probable. Thus, each parameter is randomly drawn from the uniform distribution.

6.2 Uncertainties of the Extracted Gas Prediction

The model is run for 1,000 times by using each set of parameters in Table 6-1. The length along the wellbore direction in this model is 300 feet and the length along the fracture propagation direction in this model is 600 feet. Each grid dimension is set to be 5 feet × 5 feet. Thus, there are 60 × 120 grids for each simulation. With 1,000 simulations, the data set of this model is 60 × 120 × 1,000.

In the base model, I compared the gas production from SRV region and the gas production outside the SRV region. Results have shown that nearly all extracted gas comes from the SRV region. In the uncertainty study, our discussion focuses on the depletion factors in the three selected areas.

In order to get the uncertainty of the cumulative amount of gas extracted over the 15 years for each block, the coefficient of variation is calculated. Coefficient of variation is the degree measuring the deviation of a statistical point from the mean of that statistical variable. To calculate the coefficient of variation, the mean of data and the standard deviation of data should be determined. Coefficient of variation is standard deviation multiplying 100 divided by the mean of that statistical variable.

6.2.1 Mean of Depletion Factors

Calculate the mean of the depletion factors at all locations. To do this, use the 60 x 120 x 1,000 data set and construct a 7200 x 1,000 matrix. Each column represents the depletion factor data set per simulation. With 1,000 simulations, there are 1,000 columns in the matrix. Later, calculate the mean of matrix rows and get a 7200 x 1 vector. This vector shows the mean depletion factor for each grid. Reshape this vector into a 60 x 120 matrix, then plot the heat map for the mean depletion factors over the entire 15 years (Figure 6-2).

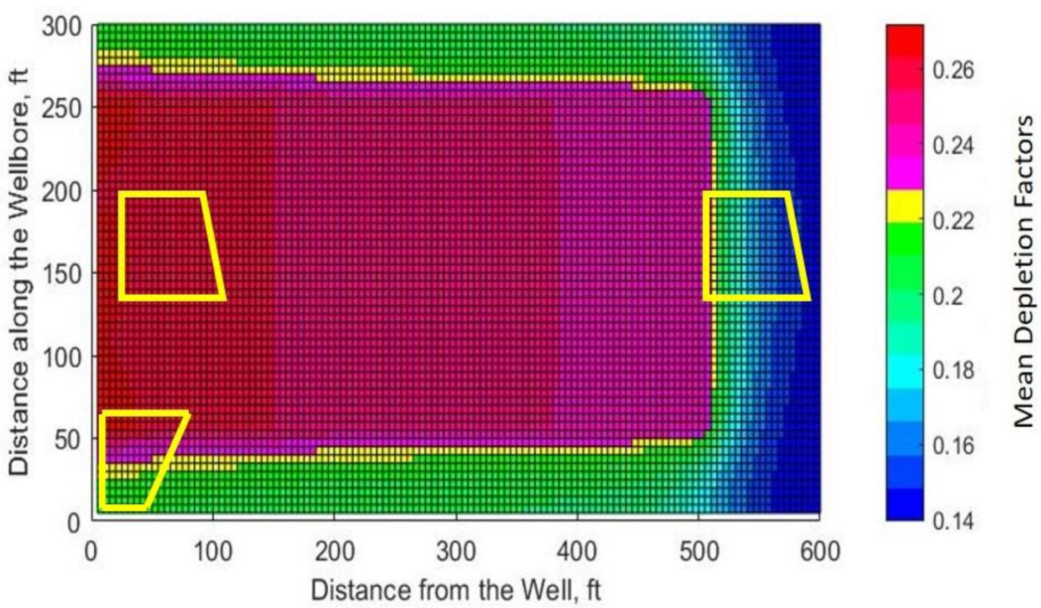

Figure 6-2. Mean of Depletion Factor at Each Location in Three Lands over 15 Years

The heat plot of mean depletion factor indicates similar results in the base model. The depletion factor decreases with the distance from the wellbore. In addition, all depletion factors inside the SRV region are greater than zero over 15 years of production, which means that all gas inside the SRV region is migratory after 15 years.

6.2.2 Standard Deviation of Depletion Factors

Once the mean depletion factor for each grid is obtained, calculate the standard deviation of those data points. Standard deviation measures the variation of a data set value. The standard deviation of the depletion factors is calculated by:

$$\text{std} = \sqrt{\frac{1}{t-1}\sum_{i=1}^{t}(DF_i - DF_m)^2} \tag{13}$$

where std is the standard deviation of depletion factor, $\{DF_1, DF_2, \ldots, DF_N\}$ are the depletion factors at each block for each simulation, DF_m is the mean value of these depletion factors and t is the number of simulation times.

Do the same matrix conversion as was done in the mean depletion factor calculation. This works out a 60 x 120 matrix which is the standard deviation of depletion factor for each grid over 15 years.

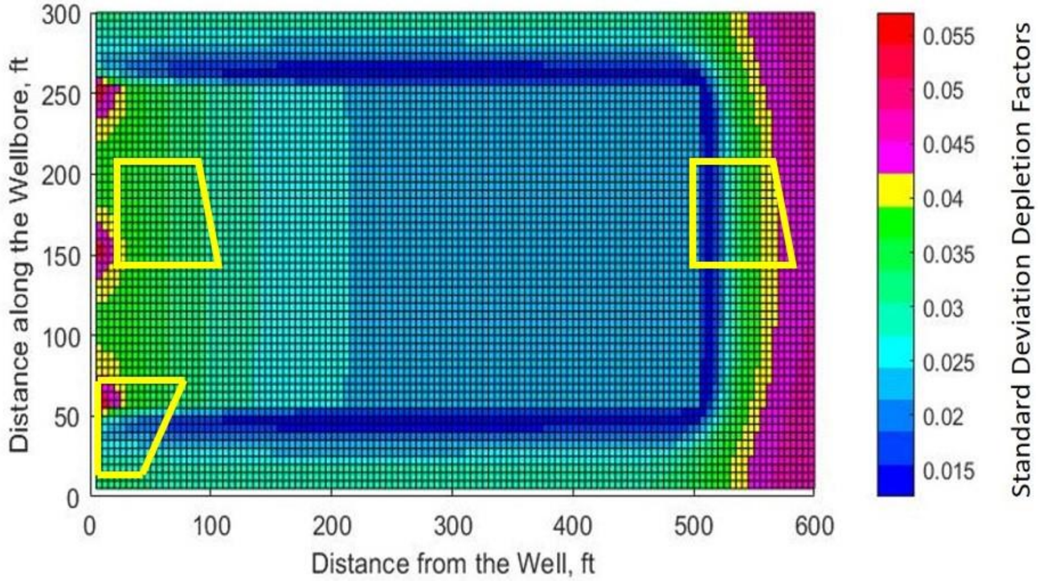

Figure 6-3. Standard Deviations of Depletion Factor at Each Location in Three Lands over 15 Years

From Figure 6-3, the maximum standard deviation is at the perforation location. The reason is that changing the bottom-hole pressure only affects the depletion of grids near the perforation clusters. Randomly changing the bottom-hole pressures adds the uncertainty to our gas predictions of the blocks adjacent to the wellbore.

6.2.3 Coefficient Variation of Depletion Factors

Coefficient of variation shows the percentage that a variable point differs from the mean of that variable data set. If the coefficient of variation is lower, the estimate has lower uncertainty. The mean and the standard deviation of depletion factor for each grid are used to find the coefficient of variation by:

$$CV = \frac{std}{DF_m} \times 100\ \% \qquad (14)$$

where CV is the coefficient of variation for each grid, std is the standard deviation, and DF_m is the mean of the depletion factor for each grid.

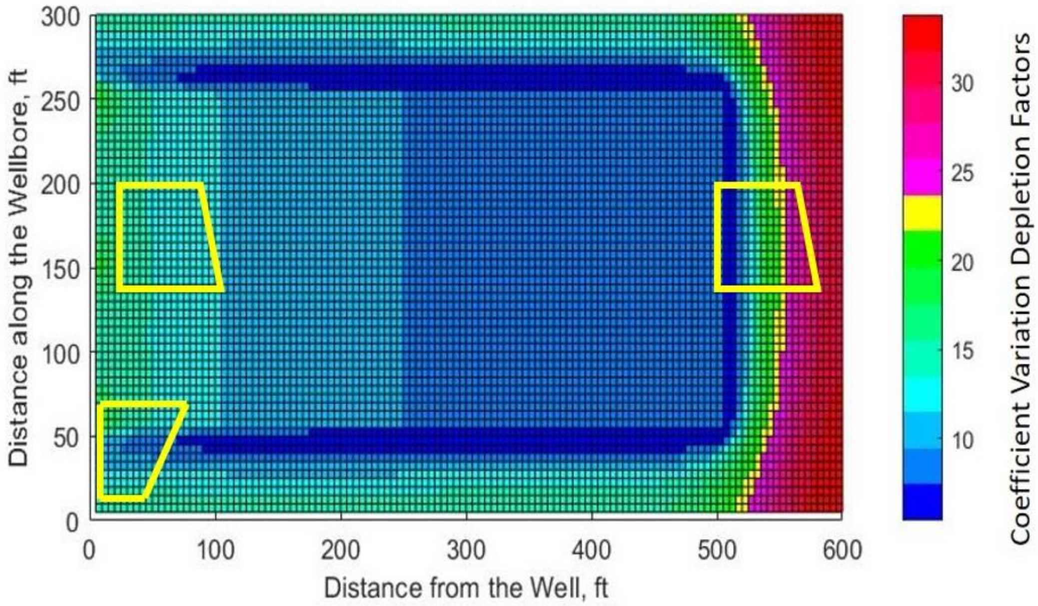

Figure 6-4. Coefficient Variations of Depletion Factor at Each Location in Three Lands over 15 Years

6.3 Capture Rule versus Trespass Rule

From each simulation, the depletion factor of each block is calculated. In Figure 6-2, Figure 6-3, and Figure 6-4, three trapezoids represent the different types of adjoining landowner areas. The trespassed gas for each block is the product of the block depletion factor times the block initial gas in place. Further, adding the trespassed gas of the blocks in the trapezoid gives the gas extraction quantity from that plot of land.

For the three plots of land described in Table 6-1, calculate the cumulative amount of natural gas over 15 years for each simulation. Consider that the sample size in the uncertainty analysis is 1,000. Area I, Area II and Area III all have a 1,000 x 1 vector that represents the extracted gas amount per simulation. The standard deviations and the coefficient variations of the extracted gas quantities from three areas are shown in Table 6-2

Table 6-3. Cumulative Gas Extracted over 15 Years for Three Plots of Land

Cumulative Gas Production, Mscf	Area I	Area II	Area III
Mean, Mscf	1229.4	1136.9	989.8
Standard Deviation, Mscf	131.2	100.2	121.3
Coefficient of Variation, %	10.7	8.8	12.3

The simulation results show that the average quantity of the extracted gas from the Area I is the greatest because most girds of Area I are in the SRV region. From Table 6-3, the coefficient variation of Area III is greater than Area I. The gas estimate from Area III has higher uncertainty. This analysis indicates that the uncertainty increases with the distance from the horizontal wellbore.

In the year of 2018, the natural gas price at Henry Hub is around 3 USD/Mscf. If the rule of trespass rule is applied, the producers should pay the Area I landowner 3,688.2 USD, the Area II landowner 3,410.7 USD and the Area III landowner 2,969.4 USD. The uncertainty of the gas estimates is about 10%. Considering the transaction fees to the lawyers and the cost of the petroleum engineering analysis, applying the rule of trespass to the Marcellus shale gas development is not worthwhile for those producers.

However, the simulation results indicate that the uniform distribution is probably not suitable for this uncertainty analysis. For example, the trespassed gas difference between the Area III and other two lands cannot be so small considering the distance of the Area III from the SRV region. The triangular distribution is recommended in this uncertainty study. On top of that, in Table 6-2, the big range of matrix permeability results in the high cumulative gas production of Area III. The cubic law can be used to adjust the matrix permeability range because the hydraulic conductivity should scale to the cubic power of the matrix aperture widths.

Chapter 7

Conclusions

The central question of this thesis is whether natural gas produced from shale using hydraulic fracturing should be subject to the capture rule or the trespass rule, which is informed by the difficulty of estimating the quantity extracted. In this thesis, I have presented a numerical reservoir base model and the results of a sensitivity analysis on the natural gas depletion factors. I have also presented a Monte Carlo simulation to quantify the uncertainty in the extracted natural gas amount from the three selected landowners' areas and consider the economic costs and benefits of calculating these quantities given the uncertainty.

The main conclusions of this study are:

Because the Stimulated Reservoir Volume (SRV) region has high fracture porosities and hydraulic conductivities, SRV region accounts for the majority of the shale gas production in the designed reservoir.

Given the dimensions of three landowner's areas, the extracted amount of natural gas from the areas are measured. However, the gas estimates have inherent high uncertainties because of the large amount of inputs in our model. The uncertainty of gas predictions increases with the land's distance from the horizontal wellbore.

Because the transaction fees and the cost of petroleum engineering analysis are likely to be greater than the value of trespassed natural gas, the rule of trespass is not justified in the context of Marcellus shale gas developments.

In spite of my claim that considering hydraulic fracturing of shale gas as a trespass action is not justified, one question remains and suggests extensions of my study. Based on the simulation analysis, the property of matrix permeability has the greatest impact on the quantity of gas extracted from three different types of adjoining land. The small gas quantity difference between three types of land results from the high range and the uniform distribution of matrix permeability. If future studies use the cubic law to adjust the range and switch to the triangular distribution, the quantity of natural gas extracted from the land adjacent to wellbore and below which is the SRV region is expected to be much greater than the land distant from wellbore and SRV region. Ultimately, this future work is likely to support the conclusion that applying the rule of trespass to the shale gas development is not convincing.

REFERENCES

Abdelmoneim, S. S., R. Rabee, A. M. Shehata, and A. Aly, 2012, Modeling Hydraulic fractures in finite difference simulators using amalgam LGR (Local Grid Refinement): Journal of Petroleum Exploration and Production Technology, v. 3(1), p. 21-35.

Ayers, K. L., K. Aminian, and S. Ameri, 2012, The impact of multistage fracturing on the production performance of the horizontal wells in shales formations: Society of Petroleum Engineers Paper No. 161347-MS, 10 p.

Belvalkar, R., and S. Oyewole, 2010, Development of Marcellus shale in Pennsylvania: Society of Petroleum Engineers Paper No. 134852-MS, 12 p.

Cipolla, C. L., E. P. Lolon, J. C. Erdle, and V. Tathed, 2009, Modeling well performance in shale-gas reservoirs: Society of Petroleum Engineers Paper No, 125532-MS, 16 p.

Cipolla, C. L., N. R. Warpinski, and M. J. Mayerhofer, 2008, Hydraulic fracture complexity: Diagnosis, remediation, and exploitation: Society of Petroleum Engineers Paper No. 115771-MS, 24 p.

Engelder, T., L. M. Cathles, and L. T. Bryndzia, 2014, The fate of residual treatment water in gas shale: Journal of Unconventional Oil and Gas Resources, v. 7, p. 33-48.

Engelder, T., and, G. G. Lash, 2008, Marcellus shale play’s vast resource potential creating stir in Appalachia: The American Oil & Gas Reporter.

Engelder, T., G. G. Lash, and R. S. Uzcátegui, 2009, Joint sets that enhance production from Middle and Upper Devonian gas shales of the Appalachian Basin: AAPG Bulletin, v. 93(7), p. 857-889

Geertsma, J., and F. de Klerk, 1969, A rapid method of predicting width and extent of hydraulically induced fractures: Journal of Petroleum Technology, v. 21(12), p. 1571-1581.

Handin, J., and, R. V. Hager Jr., 1957, Experimental deformation of sedimentary rocks under confining pressure: Tests at room temperature on dry samples: AAPG Bulletin, v. 41, p. 1-50.

Izadi, G., J. P. Junca, R. Cade, and T. Rowan, 2014, Multidisciplinary study of hydraulic fracturing in the Marcellus shale: American Rock Mechanics Association Paper No. 2014-6975, 7 p.

Kramer, B. M., and O. L. Anderson, 2005, The rule of capture – an oil and gas perspective: Environmental Law, v. 35, p. 899-954.

Lorenz, J. C., N. R. Warpinski, and L. W. Teufel, 1996, Natural fracture characteristics and effects: The Leading Edge, v. 15(8), p. 909-911.

Lueck, D., 1995, The rule of first possession and the design of the law: The Journal of Law & Economics, v. 38(2), p. 393-436.

Mayerhofer, M. J., N. A. Stegent, J. O. Barth, and K. M. Ryan, 2011, Integrating fracture diagnostics and engineering data in the Marcellus shale: Society of Petroleum Engineers Paper No. 145463-MS, 15 p.

Moghaddam, R. N., and M. Jamiolahmady, 2016, Slip flow in porous media: Fuel, v. 193, p. 298-310.

Mukherjee, H. and M. J. Economides, 1991, A parametric comparison of horizontal and vertical well performance: Society of Petroleum Engineers Paper No. 18303-PA, p. 209-216.

Nordgren, R. P., 1972, Propagation of a vertical hydraulic fracture: Society of Petroleum Engineers Journal, v. 12(4), p. 306-314.

Osholake, T. A., 2010, Factors affecting hydraulically fractured well performance in the Marcellus shale gas reservoirs: M.S. thesis, Pennsylvania State University, University Park, Pennsylvania, 99 p.

Perkins, T. K., and L. R. Kern, 1961, Widths of hydraulic fractures: Journal of Petroleum Engineers, v. 13(9), p. 937-949.

Pollard, D. D., and A. Aydin, 1988, Progress in understanding jointing over the past century: Geological Society of America Bulletin, v. 100(8), p. 1181-1204.

Roy, S., and R. Raju, 2003, Modeling gas flow through microchannels and nanopores: Journal of applied physics, v. 93(8), p. 4870-4879.

Sbar, M. L., and L. R. Sykes, 1973, Contemporary compressive stress and seismicity in eastern North America: An example of intra-plate tectonics: Geological Society of America Bulletin, v. 84, p. 1861-1881.

Soeder, D. J., 1988, Porosity and permeability of eastern Devonian gas shale: Society of Petroleum Engineers Paper No. 15213-PA, p. 116-124.

Trangenstein, J. A., and J. B. Bell, 1988, Mathematical structure of the black-oil model for petroleum reservoir simulation: SIAM J. Appl. Math, v. 49(3), p. 749-783.

Walton, I., and J. McLennan, 2013, The role of natural fractures in shale gas production: ISRM International Conference for Effective and Sustainable Hydraulic Fracturing, Brisbane, Australia, May 20-22, International Society for Rock Mechanics and Rock Engineering Paper No. ISRM-ICHF-2013-046, p. 327-356.

Warren, J. E., and P. J. Root, 1963, The behavior of naturally fractured reservoirs: Society of Petroleum Engineers Journal, v. 3(3), p. 245-255.

Witherspoon, P. A., J. S. Y. Wang, K. Iwai, and J. E. Gale, 1980, Validity of cubic law for fluid flow in a deformable rock fracture: Water Resources Research, v. 16(6), p. 1016-1024.

Zhang, T., G. S. Ellis, S. C. Ruppel, K. Milliken, and R. Yang, 2012, Effect of organic-matter type and the thermal maturity on methane adsorption in shale-gas systems: Organic Geochemistry, v. 47, p. 120-131.